Sediment sources and transport by the Kahiltna Glacier and other catchments along the south side of the Alaska Range, Alaska

A. Matmon, P. J. Haeussler, Maurice Arnold, D.L. Bourlès, Georges Aumaitre, Karim Keddadouche

Research Paper

THEMED ISSUE: Geologic Evolution of the Alaska Range and Environs

GEOSPHERE

GEOSPHERE, v. 16, no. 3

https://doi.org/10.1130/GES02190.1

10 figures; 3 tables

CORRESPONDENCE: arimatmon@mail.huji.ac.il

CITATION: Matmon, A., Haeussler, P.J., and ASTER Team, 2020, Sediment sources and transport by the Kahiltna Glacier and other catchments along the south side of the Alaska Range, Alaska: Geosphere, v. 16, no. 3, p. 787–805, https://doi.org/10.1130/GES02190.1.

Science Editor: Andrea Hampel
Guest Associate Editor: Jeffrey A. Benowitz

Received 11 August 2019
Revision received 19 January 2020
Accepted 10 February 2020

Published online 10 March 2020

Sediment sources and transport by the Kahiltna Glacier and other catchments along the south side of the Alaska Range, Alaska

A. Matmon[1], P.J. Haeussler[2], and ASTER Team[3,*]

[1]Institute of Earth Sciences, Hebrew University of Jerusalem, Jerusalem 91904, Israel
[2]U.S. Geological Survey, 4210 University Drive, Anchorage, Alaska 99508, USA
[3]Centre de Recherche et d'Enseignement de Géosciences de l'Environnement (CEREGE), UMR 6635 Centre National de la Recherche Scientifique (CNRS), Aix-Marseille University, BP 80, 13 545 Aix en Provence, Cedex 4, France

ABSTRACT

Erosion related to glacial activity produces enormous amounts of sediment. However, sediment mobilization in glacial systems is extremely complex. Sediment is derived from headwalls, slopes along the margins of glaciers, and basal erosion; however, the rates and relative contributions of each are unknown. To test and quantify conceptual models for sediment generation and transport in a simple valley glacier system, we collected samples for ^{10}Be analysis from the Kahiltna Glacier, which flows off Denali, the tallest mountain in North America. We collected angular quartz clasts on bedrock ledges from a high mountainside above the equilibrium line altitude (ELA), amalgamated clast samples from medial moraines, and sand samples from the river below the glacier. We also collected sand from nine other rivers along the south flank of the Alaska Range. In the upper catchment of the Kahiltna drainage system, toppling, rockfall, and slab collapse are significant erosional processes. Erosion rates of hundreds of millimeters per thousand years were calculated from ^{10}Be concentrations. The ^{10}Be concentrations in amalgamated samples from medial moraines showed concentrations much lower than those measured from the high mountainside, a result of the incorporation of thick, and effectively unexposed, blocks into the moraine, as well as the incorporation of material from lower-elevation nearby slopes above the moraines. The ^{10}Be sediment samples from downstream of the Kahiltna Glacier terminus showed decreasing concentrations with increasing distance from the moraine, indicating the incorporation of material that was less exposed to cosmic rays, most likely from the glacier base as well as from slopes downstream of the glacier. Taken together, ^{10}Be concentrations in various samples from the Kahiltna drainage system indicated erosion rates of hundreds of millimeters per thousand years, which is typical of tectonically active terrains. We also measured ^{10}Be concentrations from river sediment samples collected from across the south flank of the Alaska Range. Calculation of basinwide weighted erosion rates that incorporated hypsometric curves produced unrealistically high erosion rates, which indicates that the major source of sediment was not exposed to cosmic rays and was primarily derived from the base of glaciers. Moreover, the apparently high erosion rates suggest that parts of each drainage system are not in erosional steady state with respect to cosmogenic isotope accumulation.

INTRODUCTION

Geomorphologists have long recognized the important role of glaciers in shaping some of the most spectacular landscapes on Earth (e.g., Esmark, 1824), including deep fjords, rugged mountains, and broad valleys that drain vast polar ice sheets. Glaciers flowing down alpine cirques and into deep valleys create a distinctive landscape by their vigorous erosion. They produce prodigious quantities of sediment ranging from house-size boulders to fine silt. Such valley glaciers derive their sediment loads from weathering and mass wasting on adjacent slopes and from the abrasion of rock beneath (e.g., Church and Ryder, 1972; Boulton, 1996; Alley et al., 2003; MacGregor et al., 2009). One problem of glacial geomorphology is that many of the processes related to glacial erosion work beneath ice and are exceptionally difficult to observe or infer.

The specific processes of sediment mobilization in glacial systems are complex. Conceptual models describing the source for glacial sediment, the ways in which glaciers mobilize underlying sediments, and the rapidity with which they do so have been described in several studies (e.g., Bloom, 1998, figure 16-2, p. 356; Ward and Anderson, 2011; Fig. 1). For example, Bloom (1998) stated that most of the sediment transported by valley glaciers was derived from slopes of the upper glacial valley. He also described the route taken by the sediment. In that model, sediment was delivered to the glacier surface in the upper reaches of the glacier, and then gradually buried by the addition of snow, which became ice as it was buried and transported down valley. In the lower part of the glacier, where melting and ablation are dominant processes, sediment was gradually exposed to form medial and lateral moraines (Fig. 1). Ward and Anderson (2011), based on Anderson (2000) and Bozhinskiy et al. (1986), described in more detail the route taken by glacial sediment. According to their description, sediment shed from cliffs along the sides of valley glaciers was progressively buried in the accumulation zone of the glacier and became entrained in the ice. It was transported down the glacier, embedded in the ice near the margin of the glacier, until the glacier converged with another. The converging edges merged into a band of debris in the center of the combined

*ASTER Team: M. Arnold, G. Aumaître, D. Bourlès, and K. Keddadouche

glacier. This continued to move down the glacier until it crossed the equilibrium line altitude (ELA) and began to be exhumed in the ablation zone.

Upon exhumation, debris accumulates at the surface, to form the medial moraine. Once this layer of debris becomes more than a few centimeters thick, it insulates the ice beneath it from ablation (Bozhinskiy et al., 1986; Lundstrom et al., 1993). At that point, the debris-free ice nearby ablates faster than the debris-covered ice, and topography develops on top of the glacier's surface. This creates a lateral slope between debris-covered and debris-free areas, and debris migrates down this topographic slope. The exhumation rate of debris from within the ice comes into balance with the rate of removal of debris downslope, and the moraine attains a consistent thickness of debris.

During englacial transport of the debris, it is effectively entombed in ice and does not mix much from the way it fell on the surface. Certainly, some mixing may occur (Hambreky et al., 1999), but it is unlikely to be mixed with sediment other than the other debris surrounding it. Along the margins of a glacier, new debris is constantly added to the ice surface as the englacial debris from farther up the glacier translates below it, but these sources do not mix because debris that fell on the glacier farther upstream takes a deeper path through the glacier than does debris that falls farther downstream (Ward and Anderson, 2011). Based on the processes described above, Ward and Anderson (2011) argued that the concentration of cosmogenic ^{10}Be measured in any medial moraine material represents the rate at which the cliffs at the upper part of the glacier wear back.

In order to test the conceptual models for sediment generation and transport in a large and relatively simple valley glacier system, we collected samples for detailed ^{10}Be analysis from the Kahiltna Glacier, which flows off Denali (6190 m), the tallest mountain in North America. Here, we focused on the post–Last Glacial Maximum (LGM) erosion and sediment delivery of the Alaska Range drainage systems. Our sampling strategy was formulated such that it would enable us to determine the source for sediment as well as follow its route within the glacial system. Therefore, we collected clast samples in a vertical transect from a steep granitic mountainside near the head of the glacier, clasts from several medial moraines down the glacier, and river sand immediately downstream of the glacier's terminus. Using the concentration of in situ ^{10}Be as a tracer, these samples enabled us to refine our understanding of the sources and routing of glacial sediment. We then extrapolated our interpretations to the south side of the Alaska Range based on results obtained from samples collected from the outlets of other rivers that drain the south side of the Alaska Range.

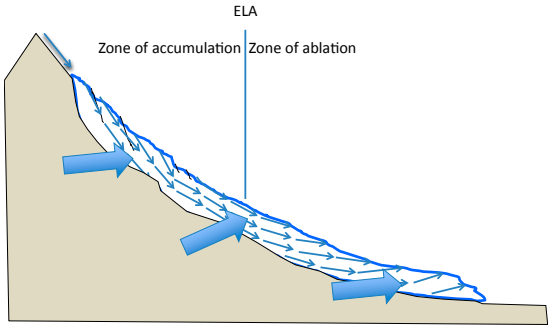

Figure 1. Conceptual description of sediment transport within a glacier, modified from Bloom (1998) and Ward and Anderson (2011). All descriptions are two-dimensional and follow a longitudinal cross section down the glacier. The major difference between previous descriptions and the one presented here is expressed by the blue thick arrows. While previous descriptions suggested that the majority of sediment is derived from the upper headwalls of the glacial system, our description indicates that the major role of sediment input is from slopes immediately above the glacier along the entire length of the glacier. This enables the incorporation of sediment with low ^{10}Be concentrations, as measured in the medial moraines. ELA—equilibrium line altitude.

Geographical and Geological Setting

The Alaska Range defines a broad arc across southern Alaska (Fig. 2) that is closely associated with a Cretaceous collision zone as well as the Denali fault (Hickman et al., 1977; Nokleberg et al., 1985; Ridgway et al., 2002; Haeussler et al., 2017a). Presently, three regions of high relief are, from west to east, the Tordrillo Mountains (3374 m), the central Alaska Range (6190 m), and the eastern Alaska Range (4216 m; Fig. 2). Rocks of the Alaska Range consist primarily of metasediments and lesser metavolcanics intruded by granitic rocks that range from Cretaceous to Paleocene–Eocene in age (e.g., Wilson et al., 2015). Uplift and topographic growth of the modern Alaska Range began at ca. 30 Ma and has been linked to the flat-slab subduction and collision of the Yakutat microplate into the southern Alaska margin (Haeussler, 2008; Haeussler et al., 2008; Benowitz et al., 2011; Finzel et al., 2011; Burkett et al., 2016). There is evidence for focused exhumation of the Tordrillo Mountains region and the Denali region, inside the bend of the Denali fault, in mid-Miocene to Pliocene time (Fitzgerald et al., 1995; Haeussler et al., 2008; Lease et al., 2016). Thus, although tectonics continue to influence the topography of the Alaska Range, the mountain range had taken form before the beginning of Pliocene time.

The climate of the Alaska Range varies on the Köppen climate classification system from tundra at the lower elevations to subarctic at the highest elevations of our samples, with local ice-cap climate only near the summits of Denali and Mount Foraker (Peel et al., 2007). Storms that impact the Alaska Range originate along the Aleutians and track to the northeast (Whiteman, 2000). Given counterclockwise atmospheric flow around low-pressure systems, the dominant wind direction is from the south, which results in a very strong rain shadow effect across the mountains. The extent of LGM glaciers was asymmetrical: Those on the south side of the range extended more than 100 km to the ocean; in contrast, glaciers on the north side of the range only extended a few tens of kilometers (Kaufman et al., 2011). Neogene glaciation in Alaska likely began around the beginning of Pliocene time, based on the oldest preserved glacial deposits along the southern Alaska margin (Eyles et al., 1991).

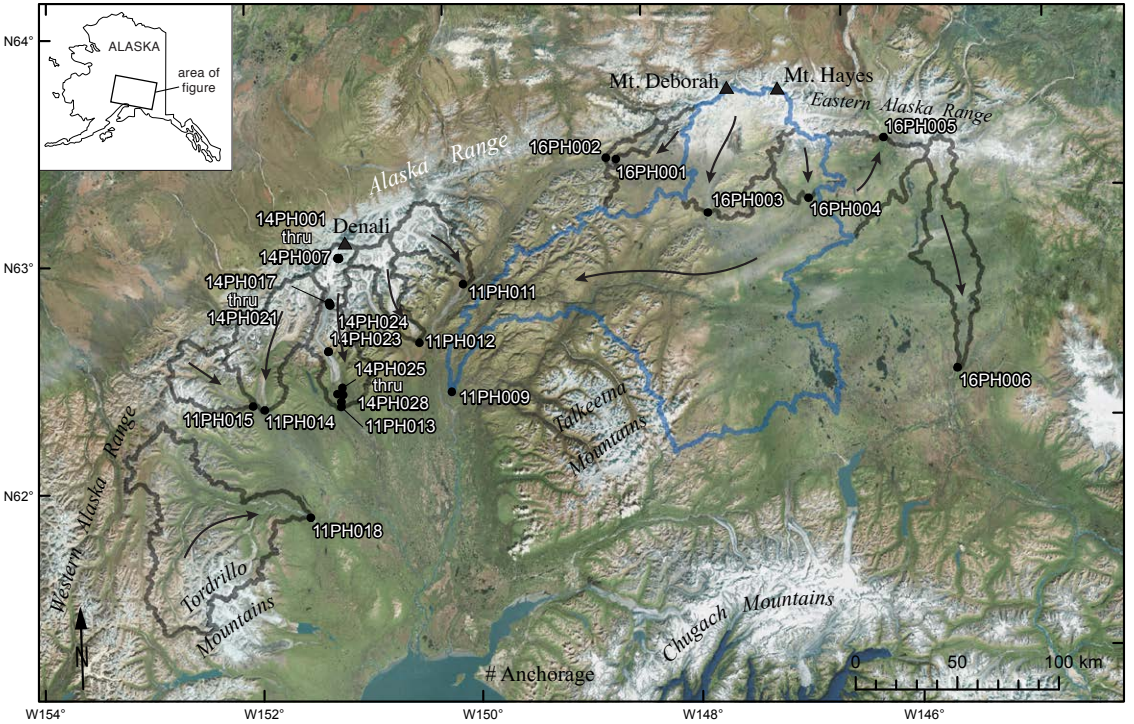

Figure 2. Overview map of the Alaska Range, showing geographic features, drainages, and sample locations. Gray lines outline catchment areas, with the exception of the large Susitna River drainage, which is outlined in blue. Black arrows show the general drainage direction within a catchment. Inset map shows location of map. Sampling sites are also shown with black dots. Background image is from ESRI World Imagery compilation (https://services.arcgisonline.com/ArcGIS/rest/services/World_Imagery/MapServer/0).

Thus, glaciation in the Alaska Range likely began around the same time. Lease (2018) used (U-Th)/He thermochronology data from both zircons and apatites to show that the rate of exhumation of the western Alaska Range increased around 4.2 Ma, which was related to landscape adjustment caused by efficient erosion associated with widespread glaciation. Prior to 4.2 Ma, erosion was slow at ≤0.3 km m.y.$^{-1}$. Erosion quickened to 1.0–1.6 km m.y.$^{-1}$ in the period between 4.2 and 2.9 Ma, and then slowed to 0.4–0.7 km m.y.$^{-1}$ since 2.9 Ma.

The bedrock along and beneath most of the Kahiltna Glacier is Cretaceous slate and graywacke turbidites, with detrital zircons as young as ca. 85 Ma (Fig. 3; Hampton et al., 2010). The turbidites have roughly similar proportions of quartz and feldspar and lesser lithic fragments (Eastham, 2002). These rocks were intruded by the McKinley series of granitic plutons around 58 Ma (Reed and Nelson, 1980; Hung, 2008). The summit of Denali and all of the taller peaks farther down the glacier consist of this granite. A large thrust fault lies along the west side of the Kahiltna Glacier in its upper reaches (Reed and Nelson, 1980; Haeussler, 2008). On the west side of the fault, there is a mixture of older Paleozoic metavolcanic and metasedimentary rocks and minor Devonian limestone intruded by 38 Ma granodiorite of the Foraker pluton (Reed and Lanphere, 1974). The Mount Foraker massif consists mostly of this granodiorite. None of these rock types, except the Foraker pluton, would be expected to contribute much quartz to the drainage system.

Our sampling scheme for the catchments was based on ease and expense of access. We focused only on catchments on the south side of the Alaska Range, as we did not want to attempt to complicate our results with variations in erosion rate due to rain shadow effects. The size of the sampled catchments varied from 649 to 4469 km^2, with an average size of 1658 km^2, except for the Susitna River catchment, which is much larger at 16,303 km^2 (Table 1).

METHODS

Thirty-one samples were collected for cosmogenic ^{10}Be analysis from southward-flowing drainage systems that discharge from the Alaska Range (Figs. 2 and 3; Table 1). Sample types were selected such that the cosmogenic isotope concentrations measured in them could be used as indicators for sediment source and route. These samples included the following:

(1) Seven samples of mixed sand and clasts were collected from bedrock ledges on the southwestern flank of the Kahiltna Peaks, a granitic

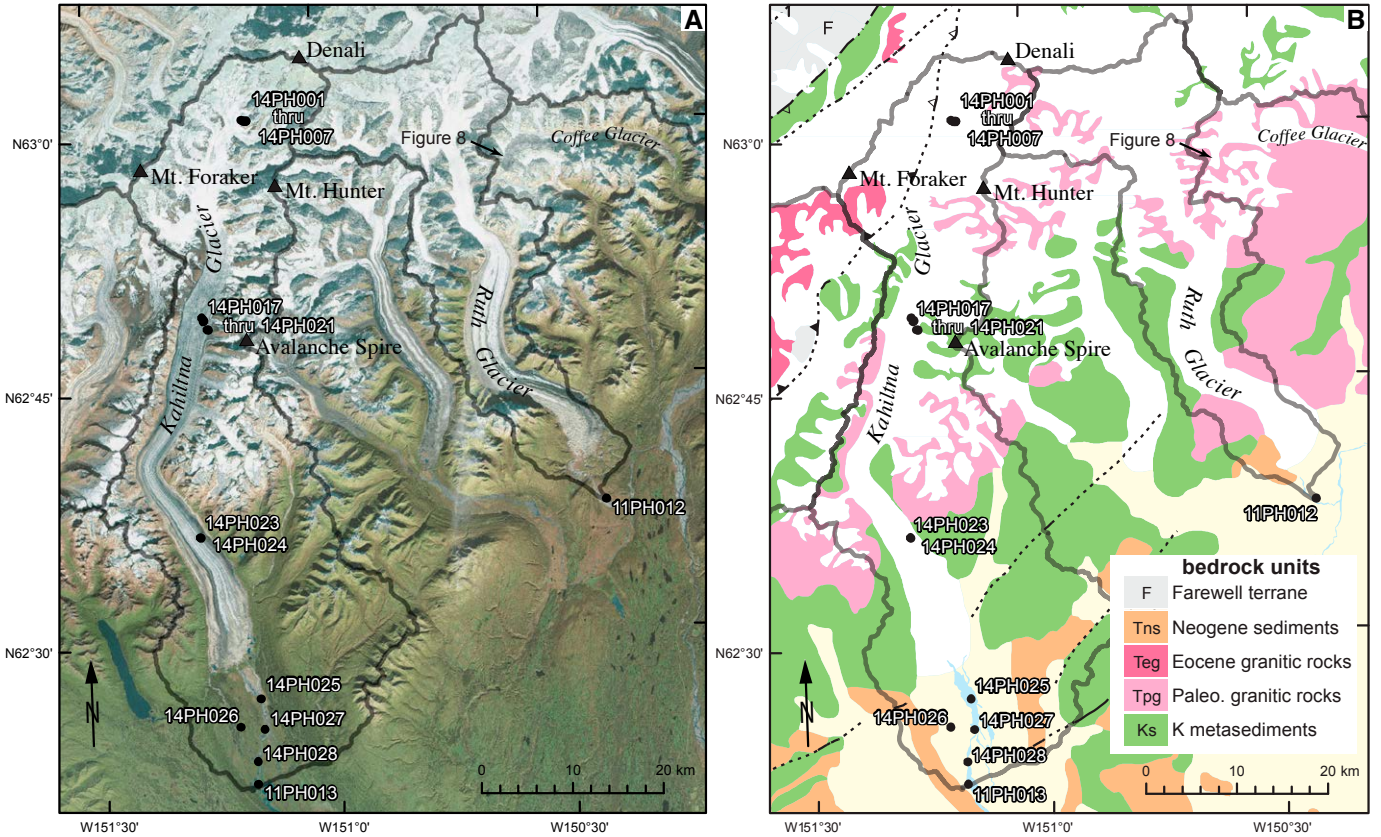

Figure 3. Map of the Kahiltna Glacier region, showing the Ruth and Coffee Glaciers, catchment boundaries (in gray), geographic features, and sample locations. (A) Satellite image showing extent of glaciers. Background image is from ESRI World Imagery compilation (https://services.arcgisonline.com/ArcGIS/rest/services/World_Imagery/MapServer/0). (B) Geologic map modified from compilation of Wilson et al. (2015). Note: Farewell terrane basement rocks consist of marble, metavolcanics, and minor metasediments. Paleo.—Paleocene; K—Cretaceous.

mountain along the east side of the Kahiltna Glacier (Figs. 3 and 4). Each sample was collected from a single ledge. Ledges ranged in elevation between 2407 and 2855 m above sea level (masl). Each sample consisted of about a liter of sand, gravel, and >100 angular and fresh clasts (up to 3 cm). The ^{10}Be concentration measured in these samples enabled us to evaluate the amount of sediment that is derived from the higher parts of the drainage system and incorporated into the glacial system.

(2) Seven samples of amalgamated clasts were collected from medial moraines on the Kahiltna Glacier west of Avalanche Spire (Figs. 3, 5, and 6). Five of these samples were collected from elevations ranging between 1377 and 1390 masl, the northernmost locations where we could safely sample the medial moraine material. Although we are not able to precisely trace each medial moraine to the source confluence, the westernmost sample (14PH018 consisting of granite) likely was sourced from the west side of Mount Hunter. The next moraine eastward (sample 14PH017) was likely sourced from the peak between Mount Hunter and Avalanche Spire. This sample consisted dominantly of granite and minor slate and graywacke with quartz veins. Samples 14PH019, 14PH020, and 14PH021 were all sourced from the basins on the north and east side of Avalanche Spire. The easternmost sampled moraine (14PH021) could be clearly traced to the confluence of glaciers at the northwestern extent of Avalanche Spire. Two additional medial moraine samples were collected at elevations of 551 and 559 masl, ~14 km north of the glacier terminus. It was not possible to trace these medial moraines northward to their

TABLE 1. GEOGRAPHICAL AND LITHOLOGICAL DATA FOR ALASKA RANGE SAMPLES

Sample name	Lat (°N)	Long (°W)	Sample elevation* (masl)	Max elevation in drainage (masl)	Geomorphic location	Geographic location	Drainage area (km²)	Distance from glacier terminus (km)	Sample composition
14PH001	63.016	151.146	2855		Mountainside	Kahiltna Peaks			Granite
14PH002	63.015	151.146	2797		Mountainside	Kahiltna Peaks			Granite
14PH003	63.015	151.147	2734		Mountainside	Kahiltna Peaks			Granite
14PH004	63.016	151.149	2678		Mountainside	Kahiltna Peaks			Granite
14PH005	63.016	151.151	2594		Mountainside	Kahiltna Peaks			Granite
14PH006	63.016	151.153	2486		Mountainside	Kahiltna Peaks			Granite
14PH007	63.017	151.156	2407		Mountainside	Kahiltna Peaks			Granite
14PH017	62.820	151.257	1390		Moraine	Kahiltna Glacier			Granite and flysch
14PH018	62.824	151.260	1394		Moraine	Kahiltna Glacier			Granite
14PH019	62.821	151.255	1392		Moraine	Kahiltna Glacier			Granite and flysch
14PH020	62.812	151.249	1369		Moraine	Kahiltna Glacier			Flysch and granite
14PH021	62.812	151.247	1377		Moraine	Kahiltna Glacier			Flysch
14PH023	62.608	151.282	551		Moraine	Kahiltna Glacier			Granite
14PH024	62.608	151.281	559		Moraine	Kahiltna Glacier			Granite
14PH025	62.447	151.166	212	6105	River	Kahiltna River		5	Sand
14PH026	62.420	151.212	213	6105	River	Kahiltna River		7	Sand
14PH027	62.417	151.161	213	6105	River	Kahiltna River		8	Sand
14PH028	62.385	151.178	217	6105	River	Kahiltna River		11	Sand
11PH013	62.363	151.180	214	6105	River	Kahiltna River	1465	14	Sand
11PH011	62.874	149.955	307	3735	River	Fountain River	844	4	Sand
11PH012	62.628	150.406	200	5685	River	Ruth River	649	4	Sand
11PH014	62.361	151.910	76	5685	River	East Fork Yentna River	1789	24	Sand
11PH015	62.378	152.020	119	2700	River	West Fork Yentna River	988	25–34	Sand
11PH018	61.883	151.513	77	3495	River	Skwentna River	4469	45	Sand
16PH001	63.375	148.378	692	2732	River	Nenana River	1221	45	Sand
16PH002	63.386	148.473	672	2732	River	Nenana River	1522	50	Sand
11PH009	62.405	150.125	104	4005	River	Susitna River	16,303	296	Sand
16PH003	63.105	147.524	773	4005	River	Susitna River	2418	33	Sand
16PH004	63.122	146.531	891	4005	River	Susitna River	917	20	Sand
16PH005	63.348	145.733	757	2683	River	Delta river	1643	31	Sand
16PH006	62.302	145.307	441	2963	River	Gakona River	1534	107	Sand

*Sample elevation is also the lowest point in each investigated drainage system (masl—meters above sea level).

source. All samples consisted of ~100 clasts, 2–5 cm across, composing a total volume of ~3 L. At each site, samples were collected by walking along 100–200 m length and 20–40 m width of the medial moraine. Where clasts consisted of flysch, only samples having quartz veins were collected. The ^{10}Be concentration measured in these samples enabled us to evaluate how much sediment in the medial moraines was derived from the higher parts of the drainage system relative to sediment eroded from nearby slopes at lower elevations.

(3) Five sediment samples were collected from the Kahiltna River downstream from the glacier terminus (Figs. 3 and 7). Each sample consisted of ~2 L of coarse sand collected across sand bars in the braid plain. The ^{10}Be concentration measured in these samples enabled us to evaluate how much sediment in the river was derived from the medial moraines relative to sediment from the base of the glacier and from the nearby slopes downstream from the glacier terminus.

(4) Twelve sediment samples were collected from eight other rivers (in addition to the Kahiltna River) that drain the south side of the Alaska Range (Figs. 2 and 7). Each sample consisted of ~1 L of coarse sand collected across sand bars in the braid plain. Samples were collected several kilometers downstream from where the rivers exit the range. Two of the 12 samples were collected from the Nenana River. Three samples were collected from the Susitna River system. Two of them were located close to

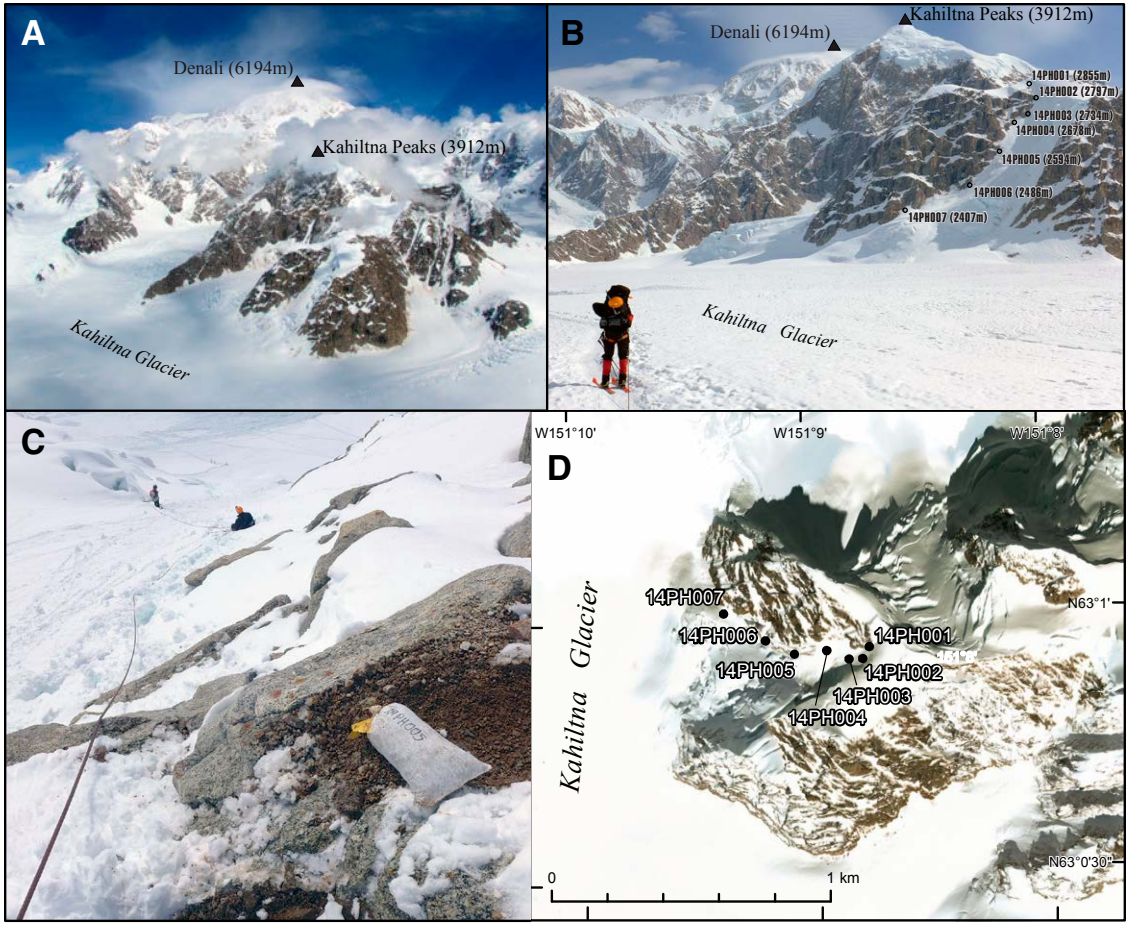

Figure 4. Photographs and locations of samples collected on the west side of the Kahiltna Peaks by Peter Haeussler (U.S. Geological Survey). See also Figure 2 for sample locations. (A) Oblique aerial view of Denali, the Kahiltna Peaks, and the area sampled. (B) View showing sample locations from Kahiltna Glacier. (C) View of one of the sampling sites, looking downward. Note numerous ledges covered with snow. Samples were collected from the gravel on the ledges. (D) Satellite image of sample locations and Kahiltna Glacier. Background image is from ESRI World Imagery compilation (https://services.arcgisonline.com/ArcGIS/rest/services/World_Imagery/MapServer/0).

the range front, and one was significantly downstream and encompassed a much larger area, which includes the Talkeetna Mountains to the south.

Samples were prepared for ^{10}Be analysis at the Cosmogenic Laboratory of The Hebrew University of Jerusalem following standard procedures (Kohl and Nishiizumi, 1992; Bierman and Caffee, 2001). Sediment samples were sieved; clast samples were first crushed and then sieved. The 250–850 mm fraction in all samples was analyzed for cosmogenic nuclide concentration measurements. All samples were analyzed for their ^{10}Be/^{9}Be ratios at the accelerator mass spectrometry (AMS) facility (ASTER) at Centre de Recherche et d'Enseignement de Géosciences de l'Environnement (CEREGE), Aix-en-Provence, France.

In the following discussion, we mainly consider the measured concentrations as tracers that indicate sediment source and sediment mixing. However, to provide broad estimates of cliff and slope erosion rates, we also consider the measured concentrations as representing steady-state erosion rates following Lal (1991) and assuming $t \gg 1/(\lambda + \mu\varepsilon)$:

$$\varepsilon = \frac{1}{\mu\left(P/N - \lambda\right)}, \quad (1)$$

where P is the production rate (atoms g^{-1} yr^{-1}), N is the measured concentration (atoms g^{-1}), μ is the absorption coefficient (cm^{-1}), which is equal to ρ/Λ, with ρ

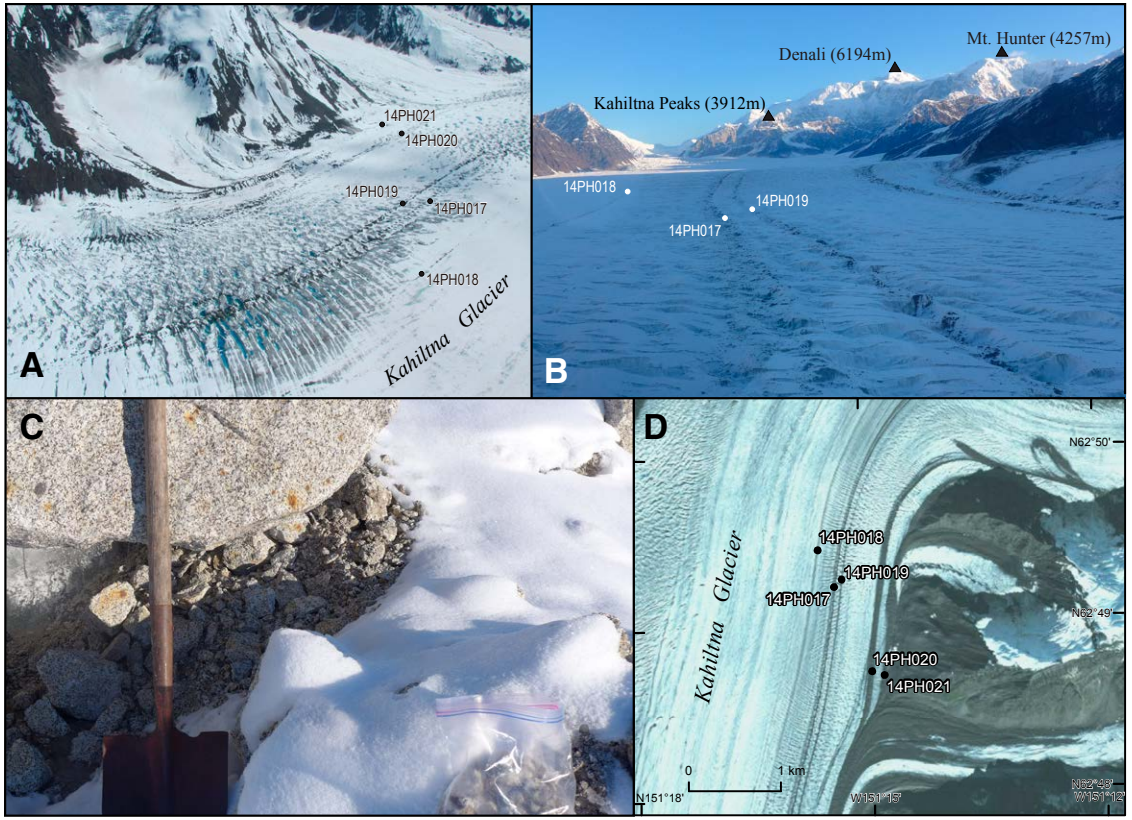

Figure 5. Photographs and locations of samples collected from the medial moraines on the Kahiltna Glacier west of Avalanche Spire. (A) Oblique aerial view of sample locations (locations approximate). (B) Aerial view of some of the sampling sites along this part of the Kahiltna Glacier (locations approximate). (C) Recent snow prior to sample collection made it difficult to see typical sample material. Here, at the margin of a boulder, the wide range of grain sizes can be seen in the granite. We only collected clasts smaller than ~4 cm. Shovel for scale. (D) Late season satellite image of sample locations. Note the moraine from which sample 14PH021 was collected. It is sourced entirely from the west side of Avalanche Spire. Note also that all the sites lie below the equilibrium line altitude (ELA). See also Figure 2 for sample locations. Satellite image is from Alaska Geospatial Imagery Services, Statewide Ortho Image Basemap (http://gis.dnr.alaska.gov/terrapixel/cubeserv/ortho?). For scale, the distance between sample locations 14PH017 and 14PH019 is 117 m.

being the target's density (g cm^{-3}) and Λ being the attenuation length (g cm^{-2}), ε is the erosion rate, and λ is the decay constant of the measured nuclide. A sea-level, high-latitude spallation production rate of 4.01 atoms g^{-1} SiO_2 yr^{-1} (Borchers et al., 2016) was used for all calculations. Production rates were scaled for latitude and altitude following Stone (2000). Muon production values and attenuation lengths were from Granger and Muzikar (2001) and Granger and Smith (2000). A neutron attenuation length of 165 g cm^{-2} and ^{10}Be decay constant of 4.99 × 10^{-7} yr^{-1} were used for all calculations (Balco et al., 2008). We applied a rock density of 2.65 g cm^{-3}. Topographic shielding corrections were applied only to the seven samples collected from the Kahiltna Peaks along the upper part of the Kahiltna Glacier (see discussion below). We assumed steady-state erosion for all samples. However, we recognize that this may not have been achieved in the high and steep granitic cliffs at the headwaters of the glacial systems. However, for sediment samples, this assumption may be reasonable (see discussion below). Nevertheless, we stress that our erosion rate calculations provide only a time-averaged order of magnitude estimate of erosion in this environment.

RESULTS AND DISCUSSION

Modes of Erosion and the Assumption of Steady State

We used the measured ^{10}Be concentrations mainly as indicators for sediment source and mixing, and as indicators for the routing of the sediment. The use of measured concentrations of cosmogenic isotopes as tracers has been successful in many environments and yielded valuable information (e.g., Clapp et al., 2001; Nichols et al., 2002, 2005; Matmon et al., 2006; Reusser and Bierman, 2010; Fruchter et al., 2011; Nelson et al., 2014; Fame et al., 2018, 2019). However, we also interpreted them in terms of average erosion rates in order

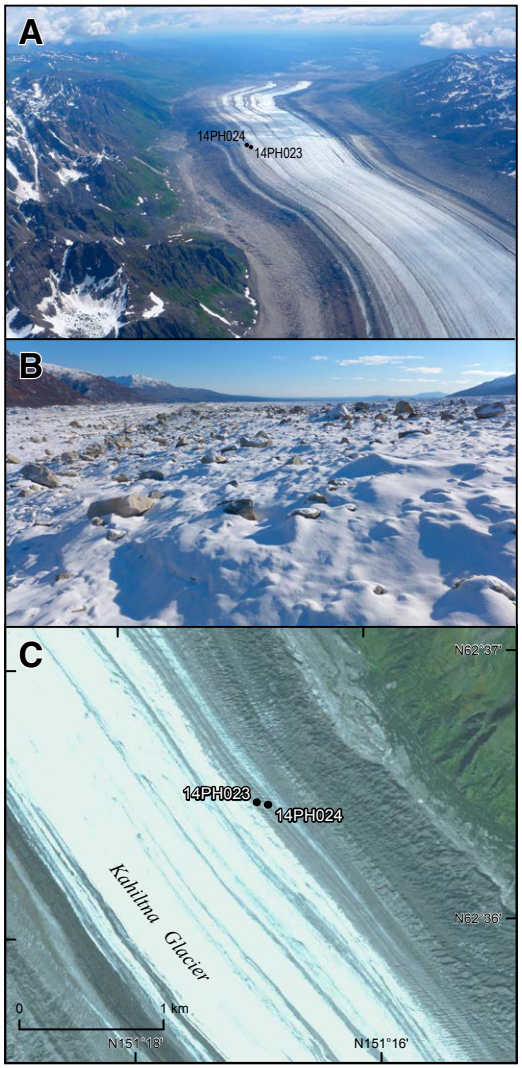

Figure 6. Photographs and locations of samples collected on the medial moraines of the lower Kahiltna Glacier by Peter Haeussler (U.S. Geological Survey). (A) Oblique aerial view of the lower Kahiltna Glacier with its many medial moraines. Note toe of glacier and the Kahiltna River in the distance. Sample locations are shown approximately. For scale, the white part of the glacier is about 1.2 km wide. (B) View on ground of sampled moraine dominated by granitic clasts. Boulders are typically greater than 1 m across. (C) Satellite image of sampling sites and numerous medial moraines. See also Figure 2 for sample locations. Satellite image is from Alaska Geospatial Imagery Services, Statewide Ortho Image Basemap (http://gis.dnr.alaska.gov/terrapixel/cubeserv/ortho?). For scale, the distance between sample locations 14PH023 and 14PH024 is 83 m.

to get a general feel of the magnitude of erosion in the region. Because glacial erosion perturbs cosmogenic nuclide depth profiles to various degrees, which may lead to erroneous calculated erosion rates (e.g., Wittmann et al., 2007; Schaller et al., 2002; Roller et al., 2013; Glotzbach et al., 2014), it is important to evaluate how close isotopic concentrations are to steady state.

When considering cosmogenic isotope concentrations in terms of erosion rates, it is assumed that ^{10}Be concentrations represent constant, long-term (generally >10^3 yr) erosion. Generally, this assumption is valid if: (1) a rock is eroded by a process that removes infinite layers continuously, and (2) a total thickness of at least 2 attenuation depths of fast neutrons has been eroded. This depth is dependent on the density of the matter being eroded. Most of the country rock being eroded within the drainage systems we sampled is composed of granite and metasedimentary rocks, all of which have a density of 2.6–2.7 g cm^{-3} (Haeussler et al., 2017b). At such densities, the typical depth of attenuation would be ~60 cm (attenuation depth = Λ/ρ). At 2 attenuation depths (~120 cm), production decreases to $1/e^2$ of the surface production rate, and the majority of cosmogenic nuclides are within that depth. In other words, once a 120 cm thickness of rock has been removed by relatively constant erosion, ^{10}Be concentrations at the surface approach steady state (e.g., Kirchner et al., 2001; Glotzbach et al., 2014).

We considered three geomorphic settings when discussing steady state:

(1) The headwall cliffs of the glacial cirque: Erosion of the resistant granitic cliffs near the headwater of the glacier on the Kahiltna Peaks occurs both by grain-by-grain erosion (as evidenced by the samples we collected on the bedrock ledges) and by toppling, rockfall, and slab collapse (Fig. 8). The concentration of ^{10}Be in sediment from this setting will depend on the thickness of the slabs and the frequency of slab detachment. Here, slabs that topple can be several meters in thickness, periodically exposing fresh rock faces that are not in isotopic steady state. Therefore, the erosion rates calculated from ^{10}Be concentrations measured in samples from the high granitic cliffs must be considered cautiously (Reinhardt et al., 2007).

(2) Slopes along the length of the glacier: For erosion rates between 100 and 600 mm k.y.$^{-1}$, typical of high and tectonically active mountain ranges (e.g., Scherler et al., 2014; Matmon et al., 2009, and references therein), 2–12 k.y. are required to remove 120 cm. This time span is shorter than the time since major post-LGM deglaciation of the region. The threshold slope for the friable metasedimentary rocks that compose most of the slopes along the length of the glacier is ~20° (Ward et al., 2012), and erosion occurs through physical weathering of small grains and clast and shallow landslides. As long as these processes are dominant, ^{10}Be concentrations will reflect the actual long-term average erosion rate (Reinhardt et al., 2007). Therefore, at high erosion rates typical of tectonically active mountain ranges, such as the Alaska Range, we assume that at least 120 cm of rock have been eroded since deglaciation, and that, with respect to ^{10}Be, concentrations approach steady state. The approach to steady state, as opposed to the actual achievement of steady state, results in overestimated erosion rates and requires a correction. Glotzbach et al. (2014) modeled this correction and showed

Figure 7. Photographs of sampling sites below the toe of the Kahiltna Glacier by Peter Haeussler (U.S. Geological Survey). (A) Oblique aerial photograph looking northwesterly toward the toe of the Kahiltna Glacier. The prominent medial moraines can be seen, as well as the region of stagnating and receding ice on the left side of the photograph. For scale, the distance between the light colored terminal moraine and the prominent stream in the lower left is about 1.7 km. (B) Looking downstream of the toe of the Kahiltna Glacier and at the headwaters of the Kahiltna River. (C) View of part of the headwaters of the Kahiltna River showing two of the sampling localities (approximately located). For scale, the distance between sample locations 14PH025 and 14PH027 is 3.4 km. (D) View toward the Kahiltna Glacier from sampling site 14PH025 on the Kahiltna River braid plain. Shovel for scale. (E) Satellite map showing sampling localities. Background image is from ESRI World Imagery compilation (https://services.arcgisonline.com/ArcGIS/rest/services/World_Imagery/MapServer/0).

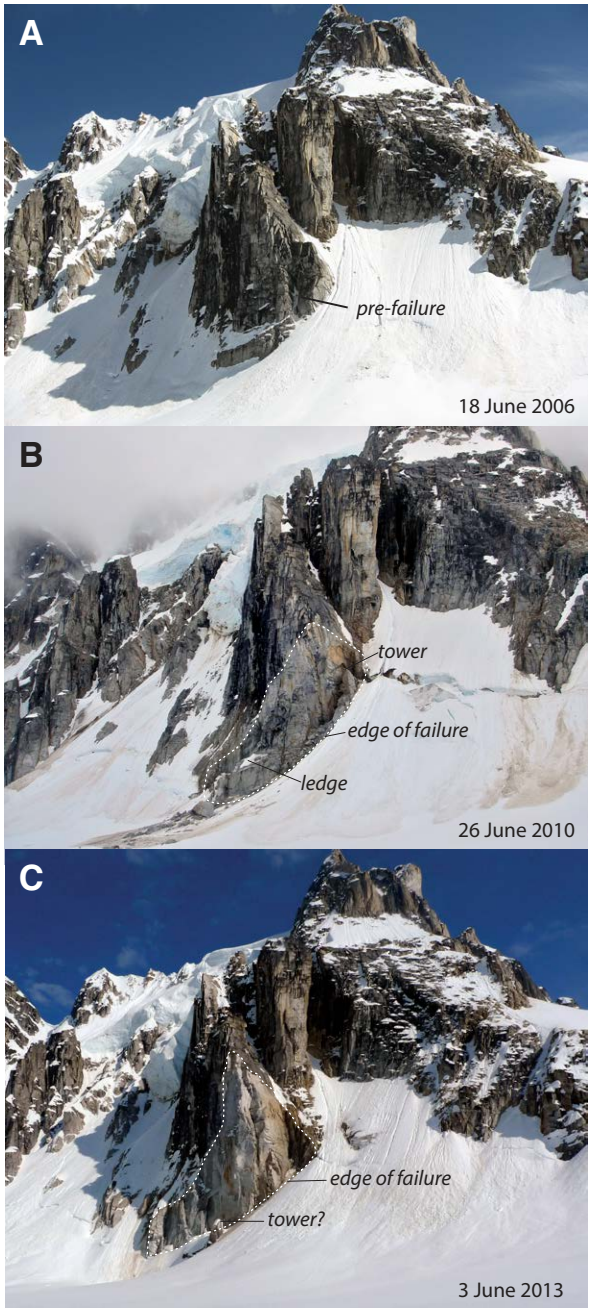

Figure 8. Sequence of photographs showing collapse of part of a rock buttress and incorporation of this material into a glacier in less than a 7 yr period. The location of this mountainside is indicated by the arrow on Figure 3, and the total height of the failure is ~300 m as shown in parts (B) and (C). Photographs are by Peter Haeussler (U.S. Geological Survey). (A) Photograph prior to buttress collapse from 18 June 2006. (B) Photograph taken during active buttress collapse on 26 June 2010. For the week we (Haeussler) were camped in this valley, there was the constant sound of falling rocks coming from this buttress. Dotted white line shows edge of failure. (C) Photograph after buttress collapse was complete (taken on 3 June 2013). Dotted white line shows edge of failure. Note this region is larger than that in 2010. No sounds of rockfall were heard coming from this area for the week that we (Haeussler) were camped there in 2013.

that for deglaciation that occurred ca. 15–10 ka and for postglaciation erosion rates that range between 100 and 600 mm k.y.$^{-1}$, corrected erosion rates are still in the hundreds of millimeters per thousand years.

(3) Outwash rivers: Here, sediment from the entire glacial basin is mixed. This includes sediment from the headwalls of cirques, sediment from slopes along the glacier, and sediment eroded from the base of the glacier, which has not been exposed to cosmic radiation. Therefore, the assumption of steady state is invalid, and the calculation of basinwide erosion rates is meaningless, regardless of whether the sample elevation or a basinwide weighted average production rate is applied for this calculation. Nevertheless, as weathering and mass wasting along the Alaska Range are likely stochastic and variable and may be influenced by specific mass-wasting events and change rapidly both in time and space, we argue that the difference in calculated erosion rates between the various drainage systems is insignificant, regardless of whether these rates were calculated considering the basin-wide weighted production rate or the sampling elevation production rate. The important outcome is that all rates, regardless of mathematical manipulations, are in the 10^2 mm k.y.$^{-1}$ magnitude and indicate rapid erosion.

Erosion near the Head of Kahiltna Glacier

The ^{10}Be concentrations in sediment samples collected from the mountainside ledges of the Kahiltna Peaks ($n = 7$) ranged between 41.1 × 10^3 ± 4.0 × 10^3 and 140.4 × 10^3 ± 7.5 × 10^3 atoms g^{-1} quartz, with an average of 78.8 × 10^3 ± 2.1 × 10^3 atoms g^{-1} quartz (Figs. 8 and 9; Table 2). They were distinctively higher than those measured in moraine and river sediment samples. Despite the presence of the adjacent and large valley glacier, we observed no glacially striated surfaces anywhere on the mountainside. Thus, although it is a glacially sculpted landscape, in detail, all surfaces have been further eroded. The granitic mountains at the head of the Kahiltna Glacier erode in two major modes: (1) continuous surface erosion and (2) toppling, rockfall, and slab collapse. Continuous surface erosion produces sediment composed of sand and gravel (as found and collected on the rock ledges). As these particles are derived from the exposed surface of the granitic cliffs, they contain the maximum possible concentration of cosmogenic nuclides and represent the

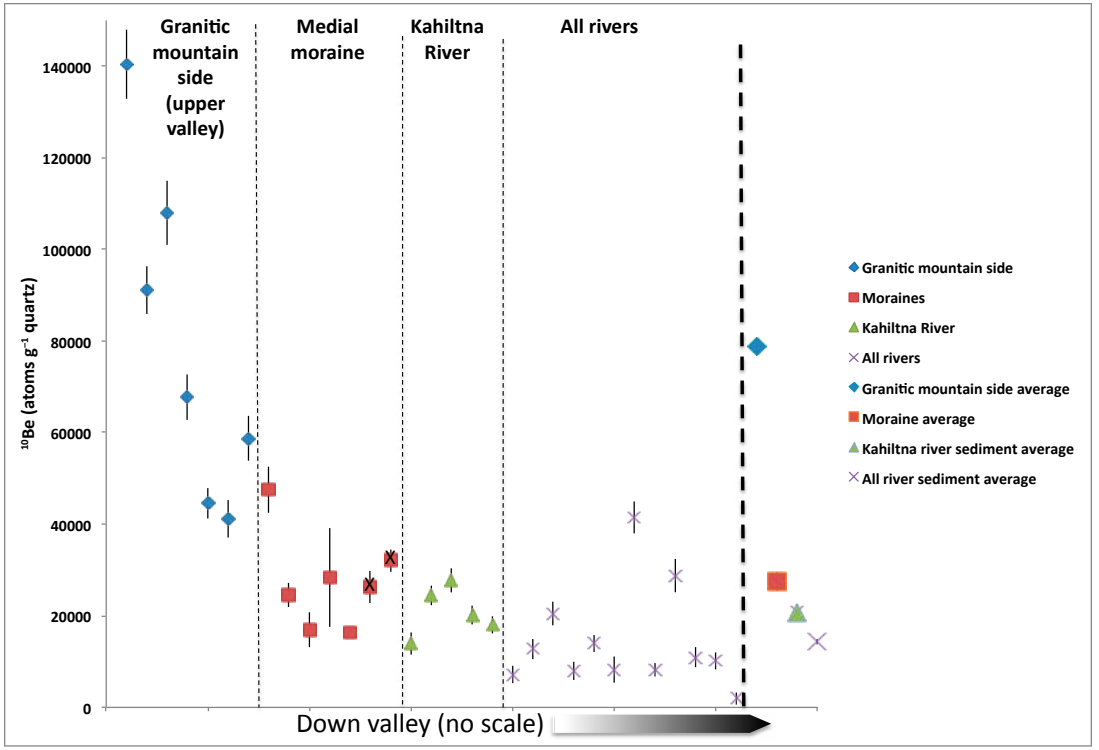

Figure 9. Measured ^{10}Be concentrations from all samples collected in this study organized by location along the drainage systems (from bedrock headwater slopes to river sediment downstream of the glaciers). Notice how concentrations decrease steadily with distance from the headwaters. Note that average values for each geomorphic group are shown to the right of the vertical bold dashed line. Moraine samples collected from the lower part of the glacier are indicated with an x.

continuous erosion of the exposed granitic surfaces. Toppling, rockfall, and slab collapse produce massive piles of sediment composed of particles ranging in size from sand to boulders. These particles are derived both from the surface of the cliffs as well as from depths of up to tens of meters (depending on the thickness of the collapsing slab). Therefore, the accumulation of cosmogenic nuclides in these particles ranges between the maximum possible to essentially zero. Sediments from both processes mix later in the medial moraine.

Each of the seven samples collected from the 500-m-tall side of the granitic Kahiltna Peaks near the head of Kahiltna Glacier represents a mix of grains that were detached from the exposed surface of the rock above the sample elevation. The pattern of ^{10}Be concentrations versus elevation (Fig. 9) indicates that the sediment on each given ledge was derived predominantly from the cliff faces immediately above the respective ledge; if the sediment had been transported downhill from ledge to ledge, mixing of sediment from different elevations would have occurred, and the lower ledges would have been covered by highly dosed sediments.

The interpretation of the seven samples collected from the granitic Kahiltna Peaks in terms of erosion rates requires the determination of the site-specific production rate of ^{10}Be. However, accurately determining the site-specific production of cosmogenic nuclides is difficult because of the amount of topographic shielding. We therefore provide three paths for erosion rate calculations (Table 3): (1) assuming no horizon shielding (i.e., shielding scaling factor = 1), (2) assuming an infinite vertical cliff above each sample (i.e., shielding scaling factor = 0.5), and (3) assuming a linear decrease in shielding from bottom to top (i.e., shielding factor changes linearly from 0.5 at the bottom to 1 at the top). In all cases, we considered the elevation of the sample for production rate calculation. The first case (shielding scaling factor = 1) provided erosion rates ranging between 178 and 481 mm k.y.$^{-1}$. The second case provided erosion rates ranging between 89 and 240 mm k.y.$^{-1}$. The third case provided erosion rates ranging between 160 and 326 mm k.y.$^{-1}$. All calculations showed extremely high erosion rates, on the order of 10^2 mm k.y.$^{-1}$, typical for tectonically active regions of high mountainous relief (e.g., Matmon et al., 2009, and references therein; Matmon and Zilberman, 2017).

The concentration versus elevation profile showed a general increase in concentration with elevation (Fig. 10). The general increase in concentrations could be partially the result of the increase of cosmogenic nuclide production

TABLE 2. LABORATORY DATA AND EROSION RATES FOR ALASKA RANGE SAMPLES

Sample name	Geomorphic location	Geographic location	Quartz (g)	Be carrier (mg)	$^{10}Be/^{9}Be$ ($\times10^{-15}$)	^{10}Be (10^3 atoms g^{-1})
14PH001	Mountainside	Kahiltna Peaks	12.221	0.18	142.61 ± 7.06	140.38 ± 7.50
14PH002	Mountainside	Kahiltna Peaks	12.362	0.266	63.39 ± 3.42	91.16 ± 5.24
14PH003	Mountainside	Kahiltna Peaks	10.984	0.2562	69.25 ± 4.29	107.95 ± 7.02
14PH004	Mountainside	Kahiltna Peaks	11.735	0.2646	44.91 ± 3.15	67.67 ± 4.93
14PH005	Mountainside	Kahiltna Peaks	14.144	0.2548	37.04 ± 2.68	44.59 ± 3.35
14PH006	Mountainside	Kahiltna Peaks	10.561	0.252	25.77 ± 2.47	41.10 ± 4.02
14PH007	Mountainside	Kahiltna Peaks	10.756	0.191	49.46 ± 3.95	58.70 ± 4.83
14PH017	Moraine	Kahiltna Glacier	8.909	0.2548	24.86 ± 2.58	47.52 ± 5.03
14PH018	Moraine	Kahiltna Glacier	12.49	0.172	26.68 ± 2.92	24.55 ± 2.73
14PH019	Moraine	Kahiltna Glacier	9.313	0.252	9.38 ± 2.10	16.96 ± 3.82
14PH020	Moraine	Kahiltna Glacier	12.812	0.212	25.68 ± 9.75	28.40 ± 10.79
14PH021	Moraine	Kahiltna Glacier	23.632	0.2618	22.20 ± 1.59	16.44 ± 1.22
14PH023	Moraine	Kahiltna Glacier	11.013	0.17	25.48 ± 3.48	26.29 ± 3.62
14PH024	Moraine	Kahiltna Glacier	11.267	0.2576	20.99 ± 1.56	32.08 ± 2.47
14PH025	River	Kahiltna River	12.705	0.252	18.47 ± 1.60	24.48 ± 2.17
14PH026	River	Kahiltna River	10.509	0.266	16.41 ± 1.54	27.75 ± 2.67
14PH027	River	Kahiltna River	11.526	0.2772	12.57 ± 1.26	20.20 ± 2.06
14PH028	River	Kahiltna River	14.179	0.2576	14.87 ± 1.54	18.06 ± 1.90
11PH013	River	Kahiltna River	18.782	0.212	18.50 ± 3.20	13.96 ± 2.43
11PH011	River	Fountain River	13.381	0.216	11.79 ± 2.00	12.74 ± 2.18
11PH012	River	Ruth River	12.605	0.214	18.09 ± 2.23	20.48 ± 2.56
11PH014	River	East Fork Yentna River	18.44	0.212	10.33 ± 2.51	7.94 ± 1.93
11PH015	River	West Fork Yentna River	15.818	0.215	15.42 ± 2.06	14.00 ± 1.89
11PH018	River	Skwentna River	8.214	0.218	4.68 ± 1.63	8.29 ± 2.89
16PH001	River	Nenana River	9.573	0.266	22.35 ± 1.83	41.51 ± 3.50
16PH002	River	Nenana River	13.094	0.2646	6.09 ± 1.16	8.23 ± 1.58
11PH009	River	Susitna River	12.925	0.215	6.41 ± 1.73	7.12 ± 1.93
16PH003	River	Susitna River	9.259	0.2604	15.29 ± 1.95	28.74 ± 3.71
16PH004	River	Susitna River	13.212	0.2688	8.06 ± 1.68	10.96 ± 2.30
16PH005	River	Delta River	10.434	0.2562	6.21 ± 1.13	10.19 ± 1.87
16PH006	River	Gakona River	11.156	0.252	1.29 ± 0.92	1.95 ± 1.39

rate with elevation. However, this is not the only factor. This is revealed by the fact that erosion rates also increase with elevation. Many studies deal with the morphologic development of glacial cirques and their relation to range topography (e.g., MacGregor, 2004; Brook et al., 2006; Sanders et al., 2010, 2012; Mitchell and Humphries, 2014; Scherler, 2014); the details of headwall retreat and variations in erosion up the headwall still warrant investigation.

Medial Moraine Material (Upper Glacier)

A 20 yr average of the modern ELA on the Kahiltna Glacier is 2104 masl, and the speed of the glacier near this location has been 195 m yr^{-1} (Burrows and Adema, 2011). However, medial moraines appear much more distinctly at elevations below ~1800 masl. Because our sampling sites were positioned close to the initial appearance of the moraines at the surface of the glacier, it is expected that the moraine sediment would be derived from the cliffs and slopes in the accumulating zone of the system. The five samples collected from medial and lateral moraines at elevations that ranged between 1369 and 1394 masl yielded ^{10}Be concentrations that ranged between $16.4 \times 10^3 \pm 1.2 \times 10^3$ and $47.5 \times 10^3 \pm 5.0 \times 10^3$ atoms g^{-1} quartz with an average of $26.8 \times 10^3 \pm 2.6 \times 10^3$ atoms g^{-1} quartz (Table 2). These concentrations are similar to those measured by Ward and Anderson (2011) on the medial moraines of glaciers in the nearby Kichatna Mountains.

The ^{10}Be concentration in the samples collected from medial moraines in the upper part of the glacier are distinctively and significantly lower than those measured from the mountainside samples (Table 2). This means that sediment produced from high elevations, with high ^{10}Be concentrations, is not a significant component of the sedimentary volume in the medial moraines.

TABLE 3. CALCULTED EROSION RATES FOR ALASKA RANGE SAMPLES

Sample name	Geomorphic location	Geographic location	Scaling factor*	^{10}Be erosion rate* (mm k.y.$^{-1}$)	Scaling factor†	^{10}Be erosion rate† (mm k.y.$^{-1}$)	Scaling factor§	^{10}Be erosion rate§ (mm k.y.$^{-1}$)
14PH001	Mountainside	Kahiltna Peaks	9.77	178.3 ± 23.9	4.90	89.0 ± 11.9	9.77	178.3 ± 23.9
14PH002	Mountainside	Kahiltna Peaks	9.44	265.3 ± 35.9	4.73	132.5 ± 18.0	8.75	254.9 ± 33.3
14PH003	Mountainside	Kahiltna Peaks	9.03	214.1 ± 29.7	4.52	106.9 ± 14.9	7.73	193.3 ± 25.5
14PH004	Mountainside	Kahiltna Peaks	8.74	330.9 ± 47.2	4.38	165.3 ± 23.6	6.71	254.0 ± 36.2
14PH005	Mountainside	Kahiltna Peaks	8.24	473.7 ± 68.1	4.13	236.7 ± 34.0	5.69	326.9 ± 47.0
14PH006	Mountainside	Kahiltna Peaks	7.71	481.0 ± 75.4	3.86	240.3 ± 37.7	4.67	291.1 ± 45.7
14PH007	Mountainside	Kahiltna Peaks	7.30	318.5 ± 47.0	3.65	159.1 ± 23.5	3.65	159.1 ± 23.5
14PH017	Moraine	Kahiltna Glacier	3.47	187.0 ± 30.3				
14PH018	Moraine	Kahiltna Glacier	3.48	363.4 ± 60.2				
14PH019	Moraine	Kahiltna Glacier	3.47	524.5 ± 134.5				
14PH020	Moraine	Kahiltna Glacier	3.42	308.0 ± 123.1				
14PH021	Moraine	Kahiltna Glacier	3.44	537.0 ± 77.0				
14PH023	Moraine	Kahiltna Glacier	1.72	167.0 ± 30.9				
14PH024	Moraine	Kahiltna Glacier	1.73	137.9 ± 20.0				
14PH025	River	Kahiltna River	1.24	129.9 ± 19.7	4.9	510.5 ± 77.2		
14PH026	River	Kahiltna River	1.24	114.6 ± 17.9	4.9	450.3 ± 70.2		
14PH027	River	Kahiltna River	1.24	157.5 ± 25.2	4.9	619.0 ± 98.8		
14PH028	River	Kahiltna River	1.26	178.0 ± 28.8	4.9	692.2 ± 11.9		
11PH013	River	Kahiltna River	1.25	228.9 ± 48.8	4.9	895.5 ± 190.9		
11PH011	River	Fountain River	1.37	274.8 ± 57.9	4.2	838.9 ± 176.7		
11PH012	River	Ruth River	1.23	153.8 ± 27.0	4.7	587.7 ± 102.9		
11PH014	River	East Fork Yentna River	1.08	349.8 ± 95.4	3.4	1094.5 ± 298.2		
11PH015	River	West Fork Yentna River	1.13	207.4 ± 37.9	2.8	504.0 ± 92.0		
11PH018	River	Skwentna River	1.09	335.4 ± 124.1	2.9	897.2 ± 331.9		
16PH001	River	Nenana River	1.94	119.6 ± 17.8	2.6	160.5 ± 23.9		
16PH002	River	Nenana River	1.91	594.2 ± 135.5	2.6	815.6 ± 185.9		
11PH009	River	Susitna River	1.11	401.7 ± 119.5	2.7	974.3 ± 287.9		
16PH003	River	Susitna River	2.08	185.4 ± 33.0	2.9	254.1 ± 45.3		
16PH004	River	Susitna River	2.31	539.7 ± 131.1	3.1	717.3 ± 174.2		
16PH005	River	Delta River	2.06	517.5 ± 114.1	2.9	734.7 ± 161.9		
16PH006	River	Gakona River	1.55	2038.2 ± 1472.6	2.4	3171.5 ± 2291.4		

Note: All calculations used a sea-level high-latitude production rate by spallation of 4.01 atoms g^{-1} yr^{-1} (Borchers et al., 2016).

*Scaling factor for mountainside samples was calculated assuming no shielding. Scaling factor for river samples was calculated considering sample elevation. Erosion rates were calculated considering the corresponding scaling factors.

†Scaling factor for mountainside samples was calculated assuming infinite vertical cliff. Scaling factor for river samples was calculated considering basin-weighted mean production. Erosion rates were calculated considering the corresponding scaling factors.

§Scaling factor for mountainside samples was calculated assuming no shielding at the topmost sample and linearly increasing the shielding to the lowermost sample, where an infinite vertical cliff was assumed.

Other sources, with much lower ^{10}Be concentrations, must supply the majority of the sediment to the medial moraine and dilute the concentration of sediment from the mountainsides. As the incorporation of subglacial sediment into medial moraines is implausible, since it is expected to appear only near the glacier's terminus, we consider two other possible sources of sediment:

(1) Sediment produced by the mix of material from headwall slab collapse, rockfall, and toppling: The ^{10}Be concentration in such mixed sediment would be controlled by the rate of continuous slope erosion, the thickness of the collapsing slab, and the production rate of cosmogenic nuclides, which would depend on latitude and elevation and the thickness of snow throughout the year. We made an unusual observation of sidewall collapse and integration of sediment into the glacier near the head of the nearby Coffee Glacier (Fig. 8). We saw that the base of a small buttress, ~200 m tall, ~100 m wide, and ~30 m thick, was removed

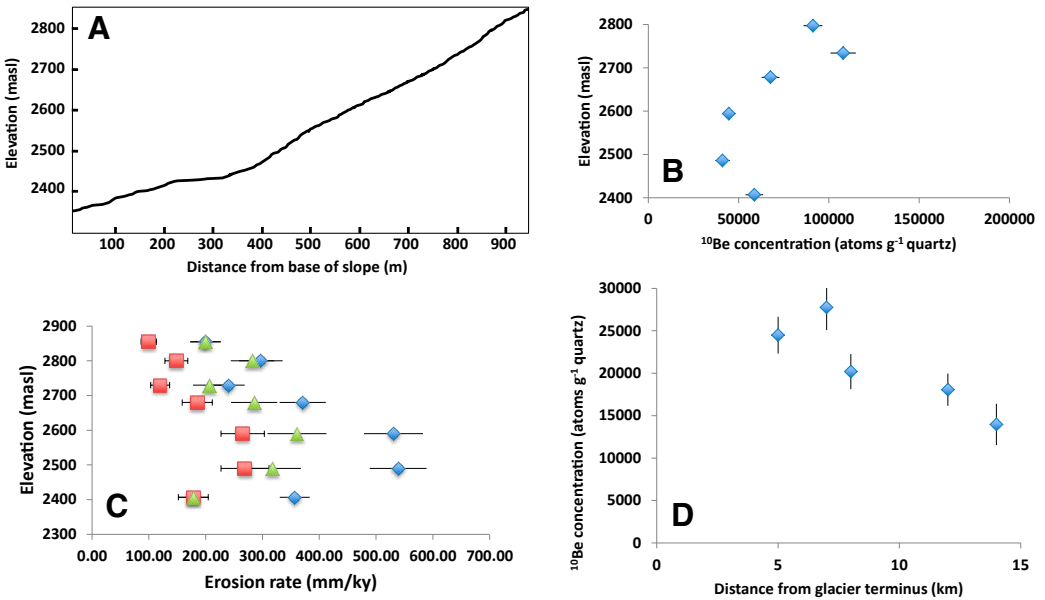

Figure 10. (A) Elevation profile of sampled granitic peaks (masl—meters above sea level). (B) ^{10}Be concentrations vs. elevation for sediment collected from ledges on the Kahiltna Peaks, near the head of the Kahiltna drainage system. (C) Erosion rates vs. elevation for sediment collected from ledges on the Kahiltna Peaks, near the head of the Kahiltna drainage system. Erosion rates were calculated three times: with topographic shielding scaling factor of 1 (solid blue diamonds), with topographic shielding scaling factor of 0.5 (solid red squares), and with a linear increase in topographic shielding scaling factor from 0.5 to 1 (solid green triangles). (D) ^{10}Be concentrations in alluvial sediment vs. distance from Kahiltna Glacier terminus. These concentrations decrease with distance from the glacier terminus.

and incorporated into the glacier in a time span of less than 7 yr. Rock fragments with high ^{10}Be concentrations from the exposed surface of the buttress would have been diluted with shielded and less-dosed rock fragments from deeper in the slab after incorporation into the margin of the glacier. Using the rock density, we calculated that a depth profile with an integrated concentration of ^{10}Be that ranges between 20,000 and 30,000 atoms g^{-1} (similar to those measured in medial moraines both in this study and by Ward and Anderson [2011]) would develop in rock slabs ranging in thickness between 40 and 450 cm.

(2) Sediment derived from mountainside slopes at elevations adjacent to the medial moraines: These slopes are mostly underlain by soft low-grade metasedimentary rock and have lower-angle slopes. The generation of sediment from these slopes with a concentration of ~26,000 atoms g^{-1} quartz, which is the average ^{10}Be concentration of the five samples collected from medial moraines at the upper part of the glacier, requires erosion rates of ~300 mm k.y.$^{-1}$. These rates are rapid but reasonable for tectonically active mountainous regions with high relief (Matmon et al., 2009, and references therein), and especially with soft and friable underlying rock. We note that these erosion rates were calculated with no topographic shielding or snow cover corrections. We applied an elevation of 1400 masl to calculate ^{10}Be production rate on these slopes.

Of the five samples collected and measured from the upper medial moraines, sample 14PH021 has the shortest distance to its source (Fig. 5). It was collected from the easternmost medial moraine, which is fed directly by debris at the confluence of the glaciers 1 km to the north (Fig. 5). Therefore, the concentration measured in sample 14PH021 ($16.4 \times 10^3 \pm 1.2 \times 10^3$ atoms g^{-1} quartz) represents the erosion of the lowest-elevation slopes in our sample suite. It yielded the lowest concentration of the five samples, with only one other medial moraine sample (14PH019) being similar to it. The rate of slope erosion required in order to supply sediment to the moraine with ^{10}Be concentration of ~16,000 atoms g^{-1} quartz, similar to that measured in sample 14PH021, is ~540 mm k.y.$^{-1}$. All the above calculated rates are only broad estimates because the actual production rate is not precisely known.

Overall, the majority of sediment supplied to the medial moraines immediately below the ELA is derived from several sources: (1) granitic peaks at the head of the Kahiltna Glacier and (2) the lower slopes around the ELA elevation. The granitic peaks erode by the infrequent collapse of slabs and continuous erosion of the granitic surfaces. These processes provide a mix of sediment with ^{10}Be concentrations that range from nearly zero in fragments that were shielded prior to collapse to the maximum possible concentration that is controlled by the elevation of the mountainside. The highly dosed material produced on exposed faces of the high mountains by continuous erosion is not a dominant sediment supplier, however. The lower slopes, around the ELA elevation, erode at hundreds of millimeters per thousand years and supply material to lateral moraines that become medial moraines downslope. The relative contribution of these two sources is hard

to evaluate since the ratio of granitic clasts versus metasedimentary clasts ranged from pure granite to pure flysch across the sampled moraines. Ward et al. (2012) discussed the influence of rock type on glacial erosion. Their discussion is relevant to the main subject of our paper in the underlying idea that friable and fractured rock (such as the metasedimentary rocks in the southern Alaska Range) erodes fast, loses mass, and produces a lot of sediment, whereas resistant granitic rock erodes slowly, maintains steep cliffs and relief, and does not produce much sediment. They reached this conclusion through morphometric analyses of the glacial valley, latitudinal and longitudinal cross sections of the glacial valley, and analysis of the threshold slope of different rock types. It should be noted that rocks exposed in their study site are the exact same rock units as found along much of the Kahiltna Glacier. The difference in erodibility of the various rock types would support our interpretation that the majority of the sediment in the medial moraine is derived from the areas in the catchment that are underlain by metasedimentary rocks and not from the high granitic cliffs. We reach this same conclusion from a totally different data set through comparing the high ^{10}Be concentrations measured in the granitic samples relative to the low concentrations measured in the medial moraine material.

Medial Moraine Material (Lower Glacier)

Down glacier from the ELA, the sedimentary cover on top of the ice increases, and the supply of sediment from the slopes adjacent to the glacier is directly observed (Fig. 5). The two medial moraine samples (14PH023 and 14PH024) from the lower glacier yielded ^{10}Be concentrations of $26.3 \times 10^3 \pm 3.6 \times 10^3$ and $32.1 \times 10^3 \pm 2.5 \times 10^3$ atoms g^{-1} quartz. The average concentration in the moraine samples from the lower part of the glacier (14PH023–14PH024; $29.2 \times 10^3 \pm 2.2 \times 10^3$ atoms g^{-1} quartz) is similar, within error, to the average concentration of the moraine samples from the upper part of the glacier (samples 14PH017–14PH021; $26.8 \times 10^3 \pm 2.6 \times 10^3$ atoms g^{-1} quartz). The significance of this similarity is that down-glacier sediment transport is rapid enough such that significant accumulation of cosmogenic nuclides does not occur in the exposed medial moraine material. If we use the Kahiltna Glacier velocity from near the ELA of 195 m yr^{-1} (Burrows and Adema, 2011), it would take ice 138 yr to transit the 27 km from the location of the highest elevation medial moraine samples to the location of the lower medial moraine samples. However, if additional material is added to medial moraines from the nearby slopes, it must be added with a dose of 20,000 and 30,000 atoms g^{-1} quartz; otherwise, it would change the overall measured concentration. We calculated the range of erosion rates of the slopes adjacent to the course of the glacier that would yield sediment with ^{10}Be concentrations of 20,000 and 30,000 atoms g^{-1} quartz. We considered the elevation of the high medial moraine samples (~1400 masl) and the elevation of the glacier terminus (~250 masl). We, therefore, estimated the erosion rates of the low-elevation slopes above the lower part of the glacier to range between 300 and 140 mm k.y.$^{-1}$. As in the case of the upper part of the glacier, slopes surrounding the glacier erode at rates of hundreds of millimeters per thousand years.

River Sediment (Downstream of the Glacier Terminus)

River sediment samples yielded the lowest ^{10}Be concentrations among the three sample groups (Fig. 9; Table 2). The five sediment samples collected from the Kahiltna River lie between 5 and 11 km below the present glacier terminus (Figs. 3 and 7). The ^{10}Be concentrations in Kahiltna River sediment samples (n = 5; 14PH025–14Ph028) ranged between $14.0 \times 10^3 \pm 2.4 \times 10^3$ and $27.8 \times 10^3 \pm 2.7 \times 10^3$ atoms g^{-1} quartz, with an average of $20.9 \times 10^3 \pm 1.0 \times 10^3$ atoms g^{-1} quartz. There was a clear trend of decreasing concentration downstream (Fig. 10). The upper two samples, 14PH025 and 14PH026, which were collected ~5 km downstream of the glacier terminus, yielded similar ^{10}Be concentrations of $24.5 \times 10^3 \pm 2.2 \times 10^3$ and $27.8 \times 10^3 \pm 2.7 \times 10^3$ atoms g^{-1} quartz, respectively. These values are similar to those measured in the medial moraines and indicate that medial moraine material may be the main source for alluvial sediment. However, at a distance of ~10 km downstream, the ^{10}Be concentrations in the alluvial sediments decreased gradually to $14.0 \times 10^3 \pm 2.4 \times 10^3$ atoms g^{-1} quartz (sample 11PH013). This decrease requires the addition of low-dosed material. As discussed above, the possibilities for the source of such low-dosed material are the low-elevation slopes on both sides of the Kahiltna River, or material that was eroded from the base of the glacier. For material derived from slopes, we calculated the range of possible slope erosion rates by considering the elevation of the glacier terminus (~250 masl) and the elevation of the samples (~215 masl). If the low-dosed sediment were derived from these low-elevation slopes, a broad estimate of the erosion rates of the low-elevation slopes above the Kahiltna River would range between 230 and 115 mm k.y.$^{-1}$.

Material derived from beneath the glacier would have eroded underneath hundreds of meters of ice and would most likely contain insignificant concentrations of ^{10}Be because of the near-zero cosmogenic nuclide production rate beneath the ice and the rapid erosion of the rock by the moving ice. This essentially unexposed sediment is the most likely source of sediment slowly mixed into the river bed load below the glacier terminus, which influences the overall measured concentration of ^{10}Be of the sediment in the river.

The calculation of basinwide average erosion rates based on the ^{10}Be concentrations measured in the Kahiltna River sediments, considering a weighted average basinwide production rate, yielded rates of ~1000 mm k.y.$^{-1}$ (Table 3). This rate obviously does not reflect the rates of erosion higher in the glaciated part of the basin, as discussed above. The reason for such a high calculated erosion rate is the combination of low ^{10}Be measured concentrations and the fact the drainage basin heads at very high elevations with high cosmogenic nuclide production rates. The unrealistically high rates suggest: (1) there is a significant contribution of undosed sediment from the base of the glacier to the river sediment, and (2) ^{10}Be concentration in outwash rivers in currently glaciated basins cannot be interpreted in terms of basinwide erosion rates. As

a whole the basin is not in erosional steady state with respect to cosmogenic nuclide accumulation.

Erosion of the Southern Flank of the Alaska Range

Several major points arise from the analysis of the Kahiltna system:

(1) The granitic mountains at the head of the glacier erode at hundreds of millimeters per thousand years. These mountains erode by continuous grain-by-grain erosion, toppling of blocks, and slab collapse. The mixed sediment from slab collapse is a significant sediment source for medial moraine material.

(2) The ^{10}Be measured concentrations and erosion rate calculations indicate that slopes at or below the ELA erode at hundreds of millimeters per thousand years, and the accumulation of cosmogenic nuclides decreases down valley as a result of the overall lowering of the ^{10}Be production rate at lower elevations. These slopes are major contributors of sediment to the glacier.

(3) Erosion beneath the glacier produces sediment that is incorporated into the fluvial system only below the terminus of the glacier.

(4) The ^{10}Be measured concentrations in the fluvial sediments immediately below the glacier are similar to those measured in the medial moraines. However, they decrease downstream as they incorporate material from beneath the glacier and from slopes adjacent to the streams.

(5) An important observation is that ^{10}Be concentrations measured in sediment samples collected from moraines and riverbeds are lower than those measured in samples collected from the mountainside of the Kahiltna Peaks. Only one river sediment sample (16PH001; $41.5 \times 10^3 \pm 3.5 \times 10^3$ atoms g^{-1} quartz) and one moraine sample (14PH017; $47.5 \times 10^3 \pm 5.0 \times 10^3$ atoms g^{-1} quartz) yielded ^{10}Be concentrations comparable to the lowest concentrations measured in Kahiltna Peaks samples (14PH005; $44.6 \times 10^3 \pm 3.3 \times 10^3$ atoms g^{-1} quartz, and 14PH006; $41.1 \times 10^3 \pm 4.0 \times 10^3$ atoms g^{-1} quartz). This pronounced difference indicates that the high granitic cliffs at the headwaters of the Kahiltna drainage system are not a major source for sediment that is later found in the medial moraines and outwash river downstream of the glacier terminus.

Given these points, we applied our understanding of erosion in the Kahiltna Glacier system to eight other drainage systems that drain the southern flank of the Alaska Range. For most of these systems, only one sediment sample was collected downstream of the glacier terminus, analogous to sample 11PH013 from the Kahiltna system. Sediment samples were collected at distances that ranged between 4 and 296 km downstream from the glacier terminus. However, apart from samples 11PH009 (296 km) and 16PH006 (107 km), samples were collected at distances less than 50 km from the glacier terminus (Table 1). The ^{10}Be concentrations in all the other river sediment samples, excluding the Kahiltna River (n = 12), ranged between $1.9 \times 10^3 \pm 1.4 \times 10^3$ and $41.5 \times 10^3 \pm 3.5 \times 10^3$ atoms g^{-1} quartz, with an average of $14.3 \times 10^3 \pm 0.7 \times 10^3$ atoms g^{-1} quartz. Omitting the outlier result from the Gakona River (sample 16PH006; $1.9 \times 10^3 \pm 1.4 \times 10^3$ atoms g^{-1} quartz) decreases the range of ^{10}Be concentrations in river sediment samples (excluding Gakona and Kahiltna Rivers) to between $7.1 \times 10^3 \pm 1.9 \times 10^3$ and $41.5 \times 10^3 \pm 3.5 \times 10^3$ atoms g^{-1} quartz, with an average of $15.5 \times 10^3 \pm 0.7 \times 10^3$ atoms g^{-1} quartz. These concentrations are slightly higher than the average ^{10}Be concentration of the five Kahiltna River samples ($20.9 \times 10^3 \pm 1.0 \times 10^3$ atoms g^{-1} quartz), but they are similar, within error, to the lowermost sediment sample of the Kahiltna River (11PH013; $14.0 \times 10^3 \pm 2.4 \times 10^3$ atoms g^{-1} quartz; Table 2).

As argued above, we infer that these concentrations provide only an order of magnitude estimate of erosion rate for each basin. When considering sample elevation, the ^{10}Be concentrations in the sediment samples correspond to erosion rates that range between 115 ± 18 and 594 ± 136 mm k.y.$^{-1}$. These results suggest, as in the case of the Kahiltna River, that slopes lower than the ELA and surrounding the glaciers and streams of these drainage systems erode at rates of hundreds of millimeters per thousand years, typical for high mountainous relief. However, when considering a weighted-average basinwide production rate, the ^{10}Be concentrations in the sediment samples (excluding the sample from Gakona River) correspond to erosion rates that range between 161 ± 24 and 1095 ± 298 mm k.y.$^{-1}$. As in the case of the Kahiltna River, we argue that the reason for such high calculated erosion rates is the combination of low ^{10}Be concentrations and the high-elevation positions of the head of these basins, which impose high cosmogenic nuclide production rates. As in the case of the Kahiltna River, we infer that undosed sediment from the base of the glacier is a major contributor to the river sediment budget. We also suggest that ^{10}Be concentration in outwash rivers in currently glaciated basins cannot be interpreted in terms of basinwide erosion rates because the entire basin is not in erosional steady state with respect to cosmogenic isotope accumulation. As weathering and mass wasting along the mountain slopes is likely stochastic and variable, we argue that the difference in calculated erosion rates between the various drainage systems is insignificant, because these high erosion rates are averaged over a very short time (low 10^3 yr) and may be influenced by specific mass-wasting events and change rapidly both in time and space. We did not find any correlation between erosion rate and basin size. This is not surprising because the overall rate of erosion along the southern front of the Alaska Range is controlled by the rate of weathering of bedrock on the slopes and mass-wasting processes that operate randomly, such that they occur equally on all slopes regardless of drainage basin size.

CONCLUSIONS

Generally, in the high mountains of the Alaska Range, the ^{10}Be concentrations in surface sediments along glaciers decrease downstream; this mainly reflects decreasing production rates with decreasing elevation. In the headwaters of the Kahiltna Glacier drainage system, the lack of preserved glacial striae on the mountainsides indicates that erosion works rapidly. Toppling,

rockfall, and slab collapse are significant erosional processes. We observed a clear relationship between ^{10}Be concentrations in sediment resting on mountainside ledges and altitude. Erosion rates of hundreds of millimeters per thousand years were calculated from these ^{10}Be concentrations, supporting the field observations.

The ^{10}Be concentrations measured in amalgamated samples from medial moraines have concentrations much lower than those measured in samples collected from the higher mountainsides. These lower ^{10}Be concentrations are partially the result of the incorporation of large blocks into the moraine that are thick enough to be effectively undosed and/or dosed at lower elevations. It's unlikely any sediment in the medial moraines is derived from undosed sediment at the base of the glacier. Furthermore, field observations also indicate the incorporation of material from the nearby slopes immediately above the moraines. The sediment samples from 5 to 11 km downstream of the Kahiltna Glacier terminus have decreasing ^{10}Be concentrations with increasing distance indicating the incorporation of additional undosed material, which is likely dominated by sediment derived from the glacier base as well as from the slopes downstream of the glacier. Taken together, ^{10}Be concentrations in various sedimentary samples from the length of the Kahiltna drainage system indicate erosion rates of hundreds of millimeters per thousand years for the various geomorphic components of the system. These rates are typical of tectonically active, high-relief terrains. The ^{10}Be concentration in samples collected from nine other rivers draining the south flank of the Alaska Range have similar concentrations to those from the upper Kahiltna River. Although our data help to broadly understand the patterns and rates of erosion of a tectonically active mountain range with large valley glaciers, we suggest that the ^{10}Be concentration in outwash rivers in currently glaciated basins cannot be interpreted in terms of basinwide erosion rates because the entire basin is not in erosional steady state with respect to cosmogenic isotope accumulation. This is because undosed sediment from the base of the glacier is a major contributor to the river sediment budget, and mass wasting along the mountain slopes is likely stochastic and variable. We argue that the difference in calculated erosion rates between the various drainage systems is insignificant because these high erosion rates are averaged over a very short time (low 10^3 yr) and may be influenced by specific mass-wasting events and change rapidly both in time and space.

ACKNOWLEDGMENTS

We thank Richard Lease and Kara Haeussler for field assistance on the Kahiltna Glacier, and Keith Labay for help in preparing the map figures. Also, thanks go to Richard Lease and Louis Sass for reviewing a previous version of the manuscript. We thank Michelle Fame, an anonymous reviewer, Guest Associate Editor Jeff Benowitz, and Andrea Hampel for very constructive reviews. Any use of trade, firm, or product names is for descriptive purposes only and does not imply endorsement by the U.S. government.

REFERENCES CITED

Alley, R.B., Lawson, D.E., Larson, G.J., Evenson, E.B., and Baker, G.S., 2003, Stabilizing feedbacks in glacier-bed erosion: Nature, v. 424, p. 758–760, https://doi.org/10.1038/nature01839.

Anderson, R.S., 2000, A model of ablation-dominated medial moraines and the generation of debris-mantled glacier snouts: Journal of Glaciology, v. 46, no. 154, p. 459–469, https://doi.org/10.3189/172756500781833025.

Balco, G., Stone, J., Lifton, N., and Dunai, T.J., 2008, A complete and easily accessible means of calculating surface exposure ages or erosion rates from ^{10}Be and ^{26}Al measurements: Quaternary Geochronology, v. 3, p. 174–195, https://doi.org/10.1016/j.quageo.2007.12.001.

Benowitz, J.A., Layer, P.W., Armstrong, P., Perry, S.E., Haeussler, P.J., Fitzgerald, P.G., and VanLaningham, S., 2011, Spatial variations in focused exhumation along a continental-scale strike-slip fault: The Denali fault of the eastern Alaska Range: Geosphere, v. 7, no. 2, p. 455–467, https://doi.org/10.1130/GES00589.1.

Bierman, P.R., and Caffee, M.W., 2001, Slow rates of rock surface erosion and sediment production across the Namib Desert and escarpment, southern Africa: American Journal of Science, v. 301, p. 326–358, https://doi.org/10.2475/ajs.301.4-5.326.

Bloom, A.L., 1998, Geomorphology (3rd ed.): Upper Saddle River, New Jersey, Prentice Hall, 482 p.

Borchers, B., Marrero, S., Balco, G., Caffee, M., Goehring, B., Lifton, N., Nishiizumi, K., Phillips, F., Schaefer, J., and Stone, J., 2016, Geological calibration of spallation production rates in the CRONUS Earth project: Quaternary Geochronology, v. 31, p. 188–198, https://doi.org/10.1016/j.quageo.2015.01.009.

Boulton, G.S., 1996, Theory of glacial erosion, transport and deposition as a consequence of subglacial sediment deformation: Journal of Glaciology, v. 42, p. 43–62, https://doi.org/10.1017/S0022143000030525.

Bozhinskiy, A., Krass, M., and Popovnin, V., 1986, Role of debris cover in the thermal physics of glaciers: Journal of Glaciology, v. 32, p. 255–266, https://doi.org/10.1017/S0022143000015598.

Brook, M.S., Kirkbride, M.P., and Brock, B.W., 2006, Cirque development in a steadily uplifting range; rates of erosion and long-term morphometric change in alpine cirques in the Ben Ohau Range, New Zealand: Earth Surface Processes and Landforms, v. 31, p. 1167–1175, https://doi.org/10.1002/esp.1327.

Burkett, C.A., Bemis, S.P., and Benowitz, J.A., 2016, Along-fault migration of the Mount McKinley restraining bend of the Denali fault defined by late Quaternary fault patterns and seismicity, Denali National Park & Preserve, Alaska: Tectonophysics, v. 693, p. 489–506, https://doi.org/10.1016/j.tecto.2016.05.009.

Burrows, R., and Adema, G., 2011, Annual Report on Vital Signs Monitoring of Glaciers in the Central Alaska Network, 2010: National Park Service, Natural Resources Program Center, Natural Resources Technical Report NPS/CAKN/NRTR 2011/423, 94 p.

Church, M., and Ryder, J.M., 1972, Paraglacial sedimentation: A consideration of fluvial processes conditioned by glaciation: Geological Society of America Bulletin, v. 83, no. 10, p. 3059–3072, https://doi.org/10.1130/0016-7606(1972)83[3059:PSACOF]2.0.CO;2.

Clapp, E.M., Bierman, P.R., Nichols, K.K., Pavich, M., and Caffee, M., 2001, Rates of sediment supply to arroyos from upland erosion determined using in situ produced cosmogenic ^{10}Be and ^{26}Al: Quaternary Research, v. 55, no. 2, p. 235–245, https://doi.org/10.1006/qres.2000.2211.

Eastham, K.R., 2002, Sedimentological and Provenance Analysis of the Upper Jurassic–Upper Cretaceous Kahiltna Assemblage: Basin Development and Tectonics of the Alaska Range Suture Zone [Master's thesis]: West Lafayette, Indiana, Purdue University, 213 p.

Esmark, J., 1824, Bidrag til vor jordklodes historie: Magazin for Naturvidenskaberne, v. 2, no. 1, p. 28–49.

Eyles, C.H., Eyles, N., and Lagoe, M.B., 1991, The Yakataga Formation: A late Miocene to Pleistocene record of temperate glacial marine sedimentation in the Gulf of Alaska, *in* Anderson, J.B., and Ashley, G.M., eds., Glacial Marine Sedimentation: Paleoclimatic Significance: Geological Society of America Special Paper 261, p. 159–180, https://doi.org/10.1130/SPE261-p159.

Fame, M.F., Owen, L.A., Spotila, J.A., Dortch, J., and Caffee, M.W., 2018, Tracking paraglacial sediment with cosmogenic ^{10}Be using an example from the northwest Scottish Highlands: Quaternary Science Reviews, v. 182, p. 20–36, https://doi.org/10.1016/j.quascirev.2017.12.017.

Fame, M.F., Owen, L.A., Spotila, L.A., and Shuster, D.L., 2019, Consistent slow exhumation in a late Cenozoic glaciated landscape: The Presidential and Carter Ranges of the White Mountains in New Hampshire, USA: Geomorphology, v. 345, 106842, https://doi.org/10.1016/j.geomorph.2019.106842.

Finzel, E.S., Trop, J.M., Ridgway, K.D., and Enkelmann, E., 2011, Upper plate proxies for flat-slab subduction processes in southern Alaska: Earth and Planetary Science Letters, v. 303, p. 348–360, https://doi.org/10.1016/j.epsl.2011.01.014.

Fitzgerald, P.G., Sorkhabi, R.B., Redfield, T.F., and Stump, E., 1995, Uplift and denudation of the central Alaska Range: A case study in the use of apatite fission track thermochronology to

determine absolute uplift parameters: Journal of Geophysical Research, v. 100, p. 20175–20191, https://doi.org/10.1029/95JB02150.
Fruchter, N., Matmon, A., Avni, Y., and Fink, D., 2011, Revealing sediment sources, mixing, and transport during erosional crater evolution in the hyperarid Negev Desert, Israel: Geomorphology, v. 134, no. 3–4, p. 363–377, https://doi.org/10.1016/j.geomorph.2011.07.011.
Glotzbach, C., Röttjer, M., Hampel, A., Hetzel, R., and Kubik, P.W., 2014, Quantifying the impact of former glaciation on catchment-wide denudation rates derived from cosmogenic ^{10}Be: Terra Nova, v. 26, p. 186–194, https://doi.org/10.1111/ter.12085.
Granger, D.E., and Muzikar, P.F., 2001, Dating sediment burial with in situ–produced cosmogenic nuclides: Theory, techniques, and limitations: Earth and Planetary Science Letters, v. 188, p. 269–281, https://doi.org/10.1016/S0012-821X(01)00309-0.
Granger, D.E., and Smith, A.L., 2000, Dating buried sediments using radioactive decay and muogenic production of ^{26}Al and ^{10}Be: Nuclear Instruments & Methods in Physics Research, Section B, Beam Interactions with Materials and Atoms, v. 172, p. 822–826, https://doi.org/10.1016/S0168-583X(00)00087-2.
Haeussler, P.J., 2008, An overview of the neotectonics of interior Alaska: Far-field deformation from the Yakutat microplate collision, *in* Freymueller, J.T., Haeussler, P.J., Wesson, R.J., and Ekstrom, G., eds., Active Tectonics and Seismic Potential of Alaska: American Geophysical Union Geophysical Monograph 179, p. 83–108, https://doi.org/10.1029/179GM05.
Haeussler, P.J., O'Sullivan, P., Berger, A.L., and Spotila, J.A., 2008, Neogene exhumation of the Tordrillo Mountains, Alaska, and correlations with Denali (Mount McKinley), *in* Freymueller, J.T., Haeussler, P.J., Wesson, R., and Ekstrom, G., eds., Active Tectonics and Seismic Potential of Alaska: American Geophysical Union Geophysical Monograph 179, p. 269–285, https://doi.org/10.1029/179GM15.
Haeussler, P.J., Matmon, A., Schwartz, D.P., and Seitz, G.G., 2017a, Neotectonics of interior Alaska and the late Quaternary slip rate along the Denali fault system: Geosphere, v. 13, p. 1445–1463, https://doi.org/10.1130/GES01447.1.
Haeussler, P.J., Saltus, R.W., Stanley, R.G., Ruppert, N., Lewis, K., Karl, S.M., and Bender, A., 2017b, The Peters Hills basin, a Neogene wedge-top basin on the Broad Pass thrust fault, south-central Alaska: Geosphere, v. 13, p. 1464–1488, https://doi.org/10.1130/GES01487.1.
Hambreky, M.J., Bennett, M.R., Dowdeswell, J.A., Glasser, N.F., and Huddart, D., 1999, Debris entrainment and transfer in polythermal valley glaciers: Journal of Glaciology, v. 45, p. 69–86, https://doi.org/10.3189/S0022143000003051.
Hampton, B.A., Ridgway, K.D., and Gehrels, G.E., 2010, A detrital record of Mesozoic island arc accretion and exhumation in the North American Cordillera: U-Pb geochronology of the Kahiltna basin, southern Alaska: Tectonics, v. 29, TC4015, https://doi.org/10.1029/2009TC002544.
Hickman, R.G., Craddock, C., and Sherwood, K.W., 1977, Structural geology of the Nenana River segment of the Denali fault system, central Alaska Range: Geological Society of America Bulletin, v. 88, p. 1217–1230, https://doi.org/10.1130/0016-7606(1977)88<1217:SGOTNR>2.0.CO;2.
Hung, C.-H., 2008, Zircon U-Pb Ages and Geochemical Characteristics of the McKinley Sequence and Associated Plutons, Central Alaska Range [M.S. thesis]: Taipei, Taiwan, National Taiwan University, 78 p.
Kaufman, D.S., Young, N.E., Briner, J.P., and Manley, W.F., 2011, Alaska palaeo-glacier atlas (version 2), *in* Ehlers, J., Gibbard, P.L., and Hughes, P.D., eds., Quaternary Glaciations—Extent and Chronology: Amsterdam, Elsevier, Developments in Quaternary Science 15, p. 427–445, https://doi.org/10.1016/B978-0-444-53447-7.00033-7.
Kirchner, J.W., Finkel, R.C., Riebe, C.S., Granger, D.E., Clayton, J.L., King, J.G., and Megahan, W.F., 2001, Mountain erosion over 10 yr, 10 k.y., and 10 m.y. time scales: Geology, v. 29, p. 591–594, https://doi.org/10.1130/0091-7613(2001)029<0591:MEOYKY>2.0.CO;2.
Kohl, C.P., and Nishiizumi, K., 1992, Chemical isolation of quartz for measurement of in-situ–produced cosmogenic nuclides: Geochimica et Cosmochimica Acta, v. 56, p. 3583–3587, https://doi.org/10.1016/0016-7037(92)90401-4.
Lal, D., 1991, Cosmic ray labeling of erosion surfaces: In situ production rates and erosion models: Earth and Planetary Science Letters, v. 104, p. 424–439, https://doi.org/10.1016/0012-821X(91)90220-C.
Lease, R.O., 2018, Pliocene erosional pulse and glacier-landscape feedbacks in the western Alaska Range: Earth and Planetary Science Letters, v. 497, p. 62–68, https://doi.org/10.1016/j.epsl.2018.06.009.
Lease, R.O., Haeussler, P.J., and O'Sullivan, P.B., 2016, Changing exhumation patterns during Cenozoic growth and glaciation of the Alaska Range: Insights from detrital thermochronology and geochronology: Tectonics, v. 35, no. 4, p. 934–955, https://doi.org/10.1002/2015TC004067.
Lundstrom, S., McCafferty, A., and Coe, J., 1993, Photogrammetric analysis of 1984–89 surface altitude change of the partially debris-covered Eliot Glacier, Mount Hood, Oregon, USA: Annals of Glaciology, v. 17, p. 167–170, https://doi.org/10.3189/S0260305500012787.
MacGregor, K.R., 2004, Glaciology and geomorphology at the mountain crest; cirque development: Eos (Transactions, American Geophysical Union), v. 85, no. 47, supplement, p. C34A–04.
MacGregor, K.R., Anderson, R.S., and Waddington, E.D., 2009, Numerical modeling of glacial erosion and headwall processes in alpine valleys: Geomorphology, v. 103, no. 2, p. 189–204, https://doi.org/10.1016/j.geomorph.2008.04.022.
Matmon, A., and Zilberman, E., 2017, Landscape evolution along the Dead Sea fault and its margins, *in* Enzel, Y., and Bar-Yosef, O., eds., The Quaternary of the Levant: Cambridge, UK, Cambridge University Press, p. 17–30, https://doi.org/10.1017/9781316106754.003.
Matmon, A., Nichols, K.K., and Finkel, R., 2006, Isotopic insights into smoothening of abandoned fan surfaces, southern California: Quaternary Research, v. 66, p. 109–118, https://doi.org/10.1016/j.yqres.2006.02.010.
Matmon, A., Simhai, O., Amit, R., Haviv, I., Porat, N., McDonald, E., Benedetti, L., and Finkel, R., 2009, Where erosion ceases: Desert pavement coated surfaces in extreme deserts present the longest-lived landforms on Earth: Geological Society of America Bulletin, v. 121, p. 688–697, https://doi.org/10.1130/B26422.1.
Mitchell, S.G., and Humphries, E.E., 2014, Glacial cirques and the relationship between equilibrium line altitudes and mountain range height: Geology, v. 43, p. 35–38, https://doi.org/10.1130/G36180.1.
Nelson, A.H., Bierman, P.R., Shakun, J.D., and Rood, D.H., 2014, Using in situ cosmogenic ^{10}Be to identify the source of sediment leaving Greenland: Earth Surface Processes and Landforms, v. 39, p. 1087–1100, https://doi.org/10.1002/esp.3565.
Nichols, K.K., Bierman, P.R., Hooke, R.L., Clapp, E.M., and Caffee, M., 2002, Quantifying sediment transport on desert piedmonts using ^{10}Be and ^{26}Al: Geomorphology, v. 45, p. 105–125, https://doi.org/10.1016/S0169-555X(01)00192-1.
Nichols, K.K., Bierman, P.R., Caffee, M., Finkel, R., and Larsen, J., 2005, Cosmogenically enabled sediment budgeting: Geology, v. 33, p. 133–136, https://doi.org/10.1130/G21006.1.
Nokleberg, W.J., Jones, D.L., and Silberling, N.J., 1985, Origin and tectonic evolution of the Maclaren and Wrangellia terranes, eastern Alaska Range, Alaska: Geological Society of America Bulletin, v. 96, p. 1251–1270, https://doi.org/10.1130/0016-7606(1985)96<1251:OATEOT>2.0.CO;2.
Peel, M.C., Finlayson, B.L., and McMahon, T.A., 2007, Updated world map of the Köppen–Geiger climate classification: Hydrology and Earth System Sciences, v. 11, p. 1633–1644, https://doi.org/10.5194/hess-11-1633-2007.
Reed, B.L., and Lanphere, M.A., 1974, Offset plutons and history of movement along the McKinley segment of the Denali fault system, Alaska: Geological Society of America Bulletin, v. 85, p. 1883–1892, https://doi.org/10.1130/0016-7606(1974)85<1883:OPAHOM>2.0.CO;2.
Reed, B.L., and Nelson, S.W., 1980, Geologic Map of the Talkeetna Quadrangle: U.S. Geological Survey Miscellaneous Field Investigations Map I-1174, 1 sheet, and 24 p., scale 1:250,000.
Reinhardt, L.J., Hoey, T.B., Barrows, T.T., Dempster, T.J., Bishop, P., and Fifield, L.K., 2007, Interpreting erosion rates from cosmogenic radionuclide concentrations measured in rapidly eroding terrain: Earth Surface Processes and Landforms, v. 32, p. 390–406, https://doi.org/10.1002/esp.1415.
Reusser, L.J., and Bierman, P.R., 2010, Using meteoric ^{10}Be to track fluvial sand through the Waipaoa River basin, New Zealand: Geology, v. 38, p. 47–50, https://doi.org/10.1130/G30395.1.
Ridgway, K.D., Trop, J.M., Nokleberg, W.J., Davidson, C.M., and Eastham, K.R., 2002, Mesozoic and Cenozoic tectonics of the eastern and central Alaska Range: Progressive basin development and deformation in a suture zone: Geological Society of America Bulletin, v. 114, p. 1480–1504, https://doi.org/10.1130/0016-7606(2002)114<1480:MACTOT>2.0.CO;2.
Roller, S., Wittmann, H., Kastowski, M., and Hinderer, M., 2013, Erosion of the Rwenzori Mountains, East African Rift, from in situ–produced cosmogenic ^{10}Be: Journal of Geophysical Research, v. 117, F03003, https://doi.org/10.1029/2011JF002117.
Sanders, J.W., Cuffey, K.M., MacGregor, K.R., Kavanaugh, J.L., and Dow, C.F., 2010, Dynamics of an alpine cirque glacier: American Journal of Science, v. 310, p. 753–773, https://doi.org/10.2475/08.2010.03.
Sanders, J.W., Cuffey, K.M., Moore, J.R., MacGregor, K.R., and Kavanaugh, J.L., 2012, Periglacial weathering and headwall erosion in cirque glacier bergschrunds: Geology, v. 40, no. 9, p. 779–782, https://doi.org/10.1130/G33330.1.
Schaller, M., von Blanckenburg, F., Veldkamp, A., Tebbens, L.A., Hovius, N., and Kubik, P.W., 2002, A 30 000 yr record of erosion rates from cosmogenic ^{10}Be in Middle European river terraces:

Earth and Planetary Science Letters, v. 204, p. 307–320, https://doi.org/10.1016/S0012-821X(02)00951-2.
Scherler, D., 2014, Climatic limits to headwall retreat in the Khumbu Himalaya, eastern Nepal: Geology, v. 42, p. 1019–1022, https://doi.org/10.1130/G35975.1.
Scherler, D., Bookhagen, B., and Strecker, M.R., 2014, Tectonic control on ^{10}Be-derived erosion rates in the Garhwal Himalaya, India: Journal of Geophysical Research, v. 119, no. 2, p. 83–105, https://doi.org/10.1002/2013JF002955.
Stone, J.O., 2000, Air pressure and cosmogenic isotope production: Journal of Geophysical Research, v. 105, p. 23753–23759, https://doi.org/10.1029/2000JB900181.
Ward, D.L., and Anderson, R.S., 2011, The use of ablation-dominated medial moraines as samplers for ^{10}Be-derived erosion rates of glacier valley walls, Kichatna Mountains, AK: Earth Surface Processes and Landforms, v. 36, p. 495–512, https://doi.org/10.1002/esp.2068.
Ward, D.J., Anderson, R.S., and Haeussler, P.J., 2012, Scaling the Teflon Peaks: Rock type and the generation of extreme relief in the glaciated western Alaska Range: Journal of Geophysical Research, v. 117, F01031, https://doi.org/10.1029/2011JF002068.
Whiteman, C.D., 2000, Mountain Meteorology: Fundamentals and Applications: Oxford, UK, Oxford University Press, 355 p.
Wilson, F.H., Hults, C.P., Mull, C.G., and Karl, S.M., compilers, 2015, Geologic Map of Alaska: U.S. Geological Survey Scientific Investigations Map 3340, pamphlet 196 p., 2 sheets, scale 1:1,584,000, http://doi.org/10.3133/sim3340.
Wittmann, H., von Blanckenburg, F., Kruesmann, T., Norton, K.P., and Kubik, P.W., 2007, Relation between rock uplift and denudation from cosmogenic nuclides in river sediment in the central Alps of Switzerland: Journal of Geophysical Research, v. 112, F04010, https://doi.org/10.1029/2006JF000729.